Learning Imbalanced Data with Beneficial Label Noise

Guangzheng Hu [1] Feng Liu [2] Mingming Gong [1] Guanghui Wang [3] Liuhua Peng [1]

Abstract

Data imbalance is a common factor hindering classifier performance. Data-level approaches for imbalanced learning, such as resampling, often lead to information loss or generative errors. Building on theoretical studies of imbalance ratio in binary classification, it is found that adding suitable label noise can adjust biased decision boundaries and improve classifier performance. This paper proposes the Label-Noise-based Re-balancing (LNR) approach to solve imbalanced learning by employing a novel design of an asymmetric label noise model. In contrast to other data-level methods, LNR alleviates the issues of informative loss and generative errors and can be integrated seamlessly with any classifier or algorithm-level method. We validated the superiority of LNR on synthetic and real-world datasets. Our work opens a new avenue for imbalanced learning, highlighting the potential of beneficial label noise. Code is available at `https://github.com/guangzhengh/LNR.git`

1. Introduction

Imbalanced data is pervasive in many real-world problems, including fraud transactions (Phua et al., 2004), disease diagnoses (Fotouhi et al., 2019), and behavioral analysis (Azaria et al., 2014). These datasets are often characterized by a high disparity in class distribution, where some classes have abundant samples while others contain very few. Such imbalance challenges traditional classifiers, which naturally require an equal sample size across classes or a sufficient number of minority class samples for effective performance (He & Garcia, 2009; Krawczyk, 2016).

[1]School of Mathematics and Statistics, University of Melbourne, Victoria, Australia [2]School of Computing and Information Systems, University of Melbourne, Victoria, Australia [3]School of Statistics and Data Science, LPMC, KLMDASR, and LEBPS, Nankai University. Correspondence to: Liuhua Peng <liuhua.peng@unimelb.edu.au>.

Proceedings of the 42^{nd} International Conference on Machine Learning, Vancouver, Canada. PMLR 267, 2025.

In practice, the minority class, often representing rare anomalies, is the focus, making accuracy an inadequate metric, especially in binary classification. Metrics like F1 score, G-mean, and Area Under the Curve (AUC) for binary classification (He & Garcia, 2009; Krawczyk, 2016), or Minority-Accuracy and Many/Medium/Few-shots for step-wise or long-tailed multi-class data, better reflect minority class performance (Cao et al., 2019; Wang et al., 2021a). This paper theoretically shows that optimizing for accuracy leads to a decision boundary in binary classification misaligned with metrics like the F1 score.

Imbalanced learning approaches can be roughly classified into **data-level** and **algorithm-level** methods. Data-level methods, such as resampling, mitigate imbalance by adding or removing samples (Kaur et al., 2019; Napierala & Stefanowski, 2016; Wang et al., 2020; 2021a) but may introduce information loss, overfitting, or generative errors. Algorithm-level methods (Chawla et al., 2004; Cao et al., 2019; Wang et al., 2021b; Li et al., 2022b) adjust learning algorithms to account for imbalance but are often tailored to specific models or problem settings, limiting their general applicability.

This paper theoretically studies how the imbalance ratio (IR) *biases* decision boundaries in binary classification with different metrics, such as accuracy and F1 score. Presentation or introduction of **label noise**, which flips sample labels to another class, can significantly alter classifier decision boundaries. Inspired by studies on **harmless** label noise (Ahfock & McLachlan, 2021; Cannings et al., 2020), which does not degrade classifier performance under certain conditions, we propose a novel Label-Noise-Re-balancing (LNR) approach that introduces artificial label noise to reallocate imbalanced class labels and thus *de-biases* the decision boundary to improve classifier performance. We further extend LNR to multi-class classification with class imbalance. As a data-level method, LNR is model-agnostic and can be seamlessly integrated with any classifier or algorithm-level approach. This flexibility enables improved performance across both binary and multi-class settings without requiring significant modifications to existing algorithms, thereby offering a robust solution to imbalanced learning.

Figure 1 illustrates the effect of adding beneficial label noise to imbalanced MNIST data with minority classes “5”, “7”,

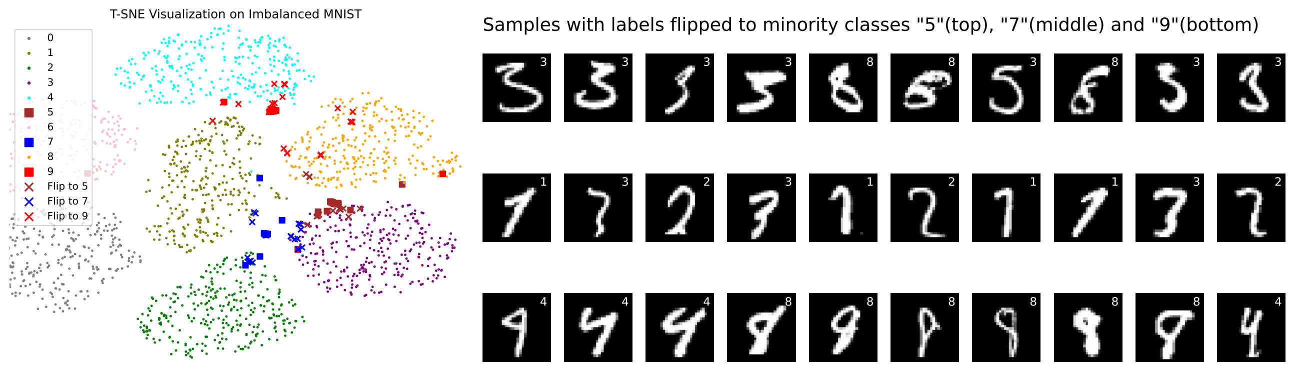

(a) T-SNE visualizations.

(b) Top-10 flipped labels into minority classes 5,7,9 by **LNR**.

Figure 1: Adding label noises to the imbalanced MNIST data. (a) shows the t-SNE visualization of the minority class (in squares) and the majority class (in dots). Noisy samples introduced by **LNR** (in crosses) are displayed in (b).

and "9". The flipped labels correspond to the top 10 samples most likely to be relabeled as each minority class. In Figure 1(a), these samples are near class boundaries, exhibiting features similar to minority class samples, as shown in Figure 1(b). Applying LNR to an extremely imbalanced MNIST dataset (30 samples per minority class, IR = 200) improved classifier accuracy from 89.93% to 94.75%.

2. Related Works and Contributions

Imbalance learning. In imbalanced binary classification, resampling is a one-shot data-level approach that balances sample sizes through under-sampling or over-sampling. To mitigate information loss from under-sampling and overfitting from over-sampling, various approaches have been proposed. Selective under-sampling methods, such as Tomek-links (Tomek, 1976), ENN (Wilson & Martinez, 2000), NCL (Li et al., 2022b), OSS (Kubat & Matwin, 2000), and ClusterCentroids (Lin et al., 2017), remove samples based on distribution characteristics. Meanwhile, synthetic over-sampling techniques, including SMOTE (Chawla et al., 2002), Borderline-SMOTE (Han et al., 2005), and ADASYN (He et al., 2008), generate new minority samples to better represent class distributions.

In multi-class classification, imbalance scenarios such as long-tailed or step-wise sample size distributions become more complex due to multiple minority classes and varying imbalance ratios. Algorithm-level methods refine loss functions or training paradigms to improve tail-class accuracy, primarily by decoupling feature learning from classifier training to separately enhance feature representation and classifier fine-tuning. Contrastive learning-based methods, including DRO-LT (Samuel & Chechik, 2021), TSC (Li et al., 2022d), BCL (Zhu et al., 2022), and SBCL (Hou et al., 2023), leverage contrastive losses during feature learning to boost feature discriminability and model robustness under imbalance. For classifier optimization, margin-based approaches like LDAM-DRW (Cao et al., 2019) and τ-norm (Kang et al., 2019) employ loss engineering to create larger decision margins for tail classes, while logit adjustment methods such as GCL (Li et al., 2022c) address softmax saturation by expanding the tail classes' embedding space through increased cloud sizes.

Data-level methods often leverage generative models or autoencoders such as Δ-encoder (Schwartz et al., 2018), DGC (Wang et al., 2020), and RSG (Wang et al., 2021a) to synthesize few-shot samples. These approaches typically depend on high-quality pre-trained models, which can introduce additional challenges, especially on scarce tail-class data, limiting the ability to generate diverse or meaningful samples. Instead of involving a generative model, Mixup (Zhang et al., 2017) interpolates features and labels via a fixed mixing ratio, empirically demonstrating its effectiveness for data augmentation. Building on this, Remix (Chou et al., 2020) introduces separate mixing ratios for features and labels to rebalance class distributions, though it retains random sampling. More recently, SelMix (Ramasubramanian et al., 2024) advanced this direction by selectively sampling pairs for mixing based on the gain on non-decomposable metrics (e.g., recall, G-mean), thereby enabling targeted improvements in specific metrics. However, SelMix's gain matrix relies on a balanced augmented auxiliary dataset. With imbalanced or small auxiliary data, the metric optimization fails to meet theoretical constraints. This limitation is notably critical in practice, where validation data is often scarce and inherently skewed–a gap our method addresses with a carefully designed noise model, which requires neither feature editing nor a balanced auxiliary dataset.

Multi-expert ensemble methods (e.g., RIDE (Wang et al., 2021b), TLC (Li et al., 2022a), and SADE (Zhang et al., 2022)) allocate specialized "experts" to model head- and tail-class features separately, achieving notable gains. While these approaches fall outside the scope of our work, they highlight the ensemble learning for tackling class imbalance.

Label noise. Instance-dependent noise (Frénay & Verleysen, 2013), where the label flip-rate (or mislabel-rate) depends on its true class and instance features, is the most general case of label noise. It is commonly assumed that samples with similar features are more likely mislabeled (Goldberger & Ben-Reuven, 2022; Song et al., 2022), particularly in the class-overlapping region. While label noise is typically harmful, with most research focusing on mitigating its impact (Goldberger & Ben-Reuven, 2022; Liu & Tao, 2015; Patrini et al., 2017; Xiao et al., 2015; Zhu et al., 2003), recent studies (Ahfock & McLachlan, 2021; Cannings et al., 2020) suggest that under certain conditions, label noise can be harmless or even beneficial. However, both works primarily focus on balanced data with symmetric label noise and do not explore how to leverage label noise to improve classifier performance for imbalanced data.

Motivation and contributions. Previous works (Ahfock & McLachlan, 2021; Cannings et al., 2020) on harmless label noise inspire the methodology to reshape decision boundaries through label noise under general models, extending from harmless to beneficial categories when addressing real-world imbalanced learning problems. It is worth mentioning that the label noise employed in this paper is asymmetric such that only the samples from the majority class have a certain probability of being flipped to the minority class, aligning with imbalanced learning. This contrasts with the symmetric label noise considered in Ahfock & McLachlan (2021); Cannings et al. (2020), where the minority samples may also be flipped to the majority class.

The main contributions of this paper are as follows: **a)** Theoretical justification of how imbalance ratio biases the decision boundary and quantification of its deviation under different evaluation metrics in binary classification. **b)** Definition of a beneficial label noise model that corrects the biased classifier's decision boundary by harmlessly reallocating imbalanced data labels. **c)** Development of a novel methodology (LNR) to introduce carefully selected beneficial label noise to imbalanced data, improving the performance of classifiers on predicting minority class samples in both binary and multi-class classification. Experiment results on synthetic and real-world data validated the superiority of our proposed method and its versatility in integrating with existing algorithm-level methods.

3. Impact of IR on Decision Boundary

In this section, we analyze the impact of the imbalance ratio (IR) on decision boundaries across various evaluation metrics in binary classification, which motivates the development of our Label-Noise-based Re-balancing (LNR) approach. Assume that two imbalanced classes have prior probabilities $\pi_1 = \Pr(Y = 1)$ and $\pi_0 = \Pr(Y = 0) = 1-\pi_1$, respectively, where $Y = 1$ refers to the minority (positive) class while $Y = 0$ represents the majority (negative) class. In the imbalanced scenario, the sample class priors satisfy $\pi_1 \ll \pi_0$ and $\mathrm{IR} = \pi_0/\pi_1$. For class $c \in \{0, 1\}$ and the sample space $\mathcal{X} \subset \mathbb{R}^d$, we denote the class-conditional distribution as $X \mid Y = c \sim P_c$ and the marginal distribution of X as $P_X(x) = \pi_1 P_1(x) + \pi_0 P_0(x)$.

3.1. Biased optimal Bayesian decision boundary by IR

Define $\eta(x) = \Pr(Y = 1 \mid X = x)$. The Bayesian decision boundary of the optimal classifier that maximizes the accuracy is defined as $S = \{x \in \mathcal{X} : \ \eta(x) = 0.5\}$.

Lemma 3.1. *The optimal Bayesian decision boundary is* $S = \{x \in \mathcal{X} : P_1(x)/P_0(x) = \pi_0/\pi_1\}$.

If the data is balanced with $\pi_0 = \pi_1$, Lemma 3.1 implies that the Bayesian decision boundary corresponds to the intersection points of $\mathrm{P}_0(x)$ and $\mathrm{P}_1(x)$. However, for imbalanced data with $\pi_1 \ll \pi_0$, the decision boundary intrudes deeply into the minority class region, increasing the risk of erroneously classifying the minority class and leading to a diminished true positive rate approaching 0. In pursuit of optimizing overall accuracy, the predictive ability of minority class samples, which is crucial in practice, is compromised. In extremely imbalanced cases, the accuracy remains high even if all samples are classified into the majority class.

Example 1. *If* $P_0 \sim N(\mu_0, \Sigma)$ *and* $P_1 \sim N(\mu_1, \Sigma)$, $S = \big\{x \in \mathcal{X} : \omega^T x + \beta = \ln(\pi_0/\pi_1)\big\}$ *with* $\omega = \Sigma^{-1}(\mu_1 - \mu_0)$ *and* $\beta = \frac{1}{2}\mu_0^T\Sigma^{-1}\mu_0 - \frac{1}{2}\mu_1^T\Sigma^{-1}\mu_1$. *For univariate normal distributions with common variance* σ^2, $S = \big\{x \in \mathcal{X} : x = \frac{1}{2}(\mu_1 + \mu_0) + \frac{\sigma^2}{\mu_1-\mu_0}\ln(\frac{\pi_0}{\pi_1})\big\}$. *If* $\pi_0 = \pi_1$, *the Bayesian decision boundary lies on the midpoint of* μ_1 *and* μ_0. *However, for imbalanced data with* $\pi_1 < \pi_0$, *the decision boundary shifts towards the minority class mean* μ_1 *as* $\ln(\pi_0/\pi_1) > 0$. *The term* $\sigma^2/(\mu_1 - \mu_0)$ *determines the relevance of the imbalance ratio* π_0/π_1 *to the deviation of the decision boundary from the midpoint, which is inversely proportional to* $\mu_1 - \mu_0$, *the class mean difference indicating the degree of class overlap.*

Lemma 3.1 is on the Bayesian decision boundary that maximizes the population-level accuracy. Similar phenomena exist in many classical classification algorithms, such as the k-nearest neighbors (KNN). We refer to Section B in the Appendix for more detailed discussions.

3.2. Impact of IR on F1 score

In many scientific applications, such as fraud detection, the predictive performance of minority class samples is often prioritized over overall accuracy. Precision and re-

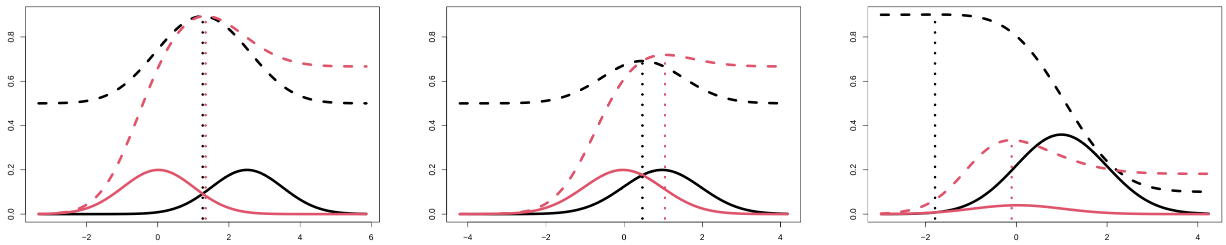

(a) $|\mu_1 - \mu_0| = 2.5, \pi_0/\pi_1 = 1$ (b) $|\mu_1 - \mu_0| = 1, \pi_0/\pi_1 = 1$ (c) $|\mu_1 - \mu_0| = 1, \pi_0/\pi_1 = 9$

Figure 2: Comparison of decision boundaries of S (vertical black dashed line) and S^{F1} (vertical red dashed line). The red solid line represents $\pi_1 \mathrm{P}_1(x)$, and the black solid line represents $\pi_0 \mathrm{P}_0(x)$. The black dashed curve represents the accuracy with respect to x, and the red dashed curve is $\mathcal{F}1(x)$.

call, defined as Precision $=$ TP$/($TP $+$ FP$)$ and Recall $=$ TP$/($TP $+$ FN$)$, are two metrics that prioritize the positive samples. Here, TP, FP, and FN represent true positives, false positives, and false negatives. Precision and recall are inversely proportional and constrained by each other. The F1 score combines precision and recall into a single metric, and it is widely used in imbalanced learning:

$$\mathrm{F1} = \frac{2 \times \text{Precision} \times \text{Recall}}{\text{Precision} + \text{Recall}} = \frac{2\mathrm{TP}}{2\mathrm{TP} + \mathrm{FP} + \mathrm{FN}}.$$

For a given classifier, TP, FP, and FN are discrete statistics based on its decision boundary. Let N be the total sample size of two classes. By the law of large numbers, as $N \to \infty$, $\mathrm{TP}/N \to \Pr(\hat{Y} = 1, Y = 1)$, $\mathrm{FP}/N \to \Pr(\hat{Y} = 1, Y = 0)$, and $\mathrm{FN}/N \to \Pr(\hat{Y} = 0, Y = 1)$ in probability, where $\hat{Y}$ is the predicted label of X with true label Y.

We consider the classifier in the form of $\hat{Y} = \mathbb{I}(\omega^T(X - x_0) > 0)$ for some $\omega \in \mathbb{R}^d$ and $x_0 \in \mathcal{X}$, here $\mathbb{I}(\cdot)$ is the indicator function. It follows that $\Pr(\hat{Y} = 1, Y = 1) = \Pr(Y = 1)\Pr(\hat{Y} = 1 \mid Y = 1) =: \pi_1 \mathcal{P}_1(x_0)$, where $\mathcal{P}_1(x_0) = \Pr(\omega^T(X - x_0) > 0 \mid Y = 1)$. In addition, $\Pr(\hat{Y} = 1, Y = 0) = \pi_0 \mathcal{P}_0(x_0)$ with $\mathcal{P}_0(x_0) = \Pr(\omega^T(X - x_0) > 0 \mid Y = 0)$ and $\Pr(\hat{Y} = 0, Y = 1) = \pi_1(1 - \mathcal{P}_1(x_0))$.

To study the impact of the imbalance ratio on the F1 score and compare its optimal decision boundary to the Bayesian decision boundary, we define a population F1 score as

$$\mathcal{F}1(x_0) = \frac{2\pi_1 \mathcal{P}_1(x_0)}{\pi_1 \mathcal{P}_1(x_0) + \pi_0 \mathcal{P}_0(x_0) + \pi_1}. \tag{1}$$

Lemma 3.2. *The decision boundary that maximizes $\mathcal{F}1(x_0)$ for $x_0 \in \mathcal{X}$ is*

$$S^{\mathrm{F1}} = \left\{ x_0 \in \mathcal{X} : \frac{P_1(x_0)}{P_0(x_0)} = \frac{\mathcal{F}1(x_0)}{2 - \mathcal{F}1(x_0)} \frac{\pi_0}{\pi_1} \right\}.$$

The proof of Lemma 3.2 implies $\eta(x_0) = 0.5 \times \mathcal{F}1(x_0)$ for $x_0 \in S^{\mathrm{F1}}$, indicating that the probability of x_0 belongs to the positive class is half of the maximum population F1 score on the decision boundary. Consequently, the optimal F1 score decision boundary coincides with the optimal Bayesian decision boundary when $\mathcal{F}1(x_0) = 1$ for $x_0 \in S^{\mathrm{F1}}$. In such case, $\Pr(\hat{Y} = 1, Y = 0) = \Pr(\hat{Y} = 0, Y = 1) = 0$, indicating full separability between the two classes.

However, when class overlap exists such that $\mathcal{F}1(x_0) < 1$, we observe $P_1(x_0)/P_0(x_0) < P_1(x)/P_0(x)$ for $x_0 \in S^{\mathrm{F1}}$ and $x \in S$. This shows that the optimal F1 score decision boundary deviates from the optimal Bayesian decision boundary. The discrepancy between S and S^{F1} is linked to $\frac{\mathcal{F}1(x_0)}{2-\mathcal{F}1(x_0)}$, which becomes severe when the maximum F1 score decreases. In addition, this term is weighted by the imbalance ratio π_0/π_1, further amplifying the deviation.

Lemma 3.2 indicates that for $x_0 \in S^{\mathrm{F1}}$, the maximum F1 score satisfies $\frac{\mathcal{F}1(x_0)}{2-\mathcal{F}1(x_0)} = \frac{P_1(x_0)}{P_0(x_0)} \frac{\pi_1}{\pi_0}$, which decreases as the π_1/π_0 decreases. Consequently, the optimal F1 score decreases as the imbalance ratio becomes more severe, limiting the best performance of classifiers in terms of the F1 score. In addition, optimizing accuracy under an imbalance ratio would further sacrifice the F1 score.

Example 2. *Figure 2 exhibits the relationship between the deviation of S and S^{F1} with the imbalance ratio π_0/π_1 and the class overlap $|\mu_1 - \mu_0|$ when $P_0 \sim N(\mu_0, \sigma^2)$ and $P_1 \sim N(\mu_1, \sigma^2)$. In Figure 2(a), with balanced data and small class overlap, the deviation between the optimal accuracy and the maximum F1 score is negligible, and the decision boundaries align closely. In Figure 2(b), the deviation increases with larger class overlap. In Figure 2(c), the deviation grows with an increasing imbalance ratio, with a lower F1 score at the Bayesian decision boundary.*

Although some of prior studies (Saerens et al., 2002; Xu et al., 2021) share similar findings on how the imbalance ratio impacts the decision boundaries, our theoretical analysis on misaligned optimal decision boundaries that maximize accuracy and F1-score provides a deeper insight that motivates us in proving the counteracted impact of asymmetric instance-dependent label noise model on decision boundaries under class imbalance.

4. Label-Noise-based Re-balancing Approach

Motivated by the decision boundary distortion due to class imbalance, we propose a novel Label-Noise-Re-balancing (LNR) approach. By introducing beneficial asymmetric label noise, LNR improves classification performance in both binary and multi-class imbalanced learning.

4.1. Methodology

The proposed LNR method consists of two steps: (1) introduce artificial label noises to the original data, and (2) train a classifier on the noisy data. We first focus on binary classification to motivate and justify the introduction of label noise, which plays a crucial role in correctly adjusting the decision boundary on the relabeled data.

Suppose the original data $(X, Y) \sim \mathrm{P}$. Define $\rho(x) = \Pr(Y^* = 1 \mid X = x, Y = 0)$ as the probability of flipping a sample from the true label $Y = 0$ to the noisy label $Y^* = 1$, similarly, define $\gamma(x) = \Pr(Y^* = 0 \mid X = x, Y = 1)$. With the flipped labels, we obtain the noisy data pairs $(X, Y^*) \sim \mathrm{P}^*$. Consequently, $\eta^*(x) = \Pr(Y^* = 1 \mid X = x) = \eta(x)[1 - \gamma(x)] + [1 - \eta(x)]\rho(x)$.

The label noises discussed in Ahfock & McLachlan (2021); Cannings et al. (2020) are symmetric and proportional to classification difficulty $\eta(x)$, where both positive and negative samples are equally likely to be flipped on the decision boundary. The classifier remains consistent on such symmetric label noises, counterbalancing the distortion and leaving the decision boundary unchanged. For example, with $\rho(x) = \eta(x), \rho(x) + \gamma(x) = 1$, we have $\eta^*(x) = \eta(x)$, making the noise model harmless.

However, in imbalanced data, the overwhelming number of majority class samples invading the minority class region often results in significant misclassification of minority class samples. To achieve a higher F1 score by adjusting the decision boundary and reducing the imbalance ratio near the decision boundary, we consider an asymmetric label noise model that only flips majority class samples to minority class samples. This approach shifts the biased decision boundary toward the majority class region rather than neutralizing the shifts with symmetric noise. Since deeply invaded majority class samples cause greater harm, we aim for a noise model directly proportional to the extent of this invasion. Therefore, we propose the flipped rates satisfy:

$$\rho(x) \propto \eta(x), \quad \gamma(x) = 0. \tag{2}$$

Using this label noise model, we can generate the noisy data, as outlined in Algorithm 1. As an example shown in Figure 3, the asymmetric label noise model pushes the biased decision boundary (left vertical dashed line) on imbalanced data distribution (solid curves) toward the majority region at the corrected decision boundary (right vertical dashed line) on the data distribution with label noises (dashed curves).

By introducing artificial label noises with a well-behaved flip-rate function $\rho(x)$, the deviation of the decision boundary caused by asymmetric label noise can correct the biased decision boundary on imbalanced data. The flipped majority class samples enrich the minority class while simultaneously reducing the number of the majority class. The Bayesian decision boundary that maximizes accuracy based on the relabeled sample (X, Y^*) is $S^* = \{x^* \in \mathcal{X} : \eta^*(x^*) = 0.5\}$.

Lemma 4.1. *The optimal Bayesian decision boundary based on (X, Y^*) is*

$$S^* = \left\{ x^* \in \mathcal{X} : \frac{P_1(x^*)}{P_0(x^*)} = [1 - 2\rho(x^*)]\frac{\pi_0}{\pi_1} \right\},$$

conditional on that the flip-rate on the decision boundary satisfies $\rho(x^*) < 0.5$

As $1 - 2\rho(x^*) < 1$, Lemma 4.1 indicates that the Bayesian decision boundary on noisy data shifts back to the majority class region. While this may sacrifice some overall accuracy, it improves the classification accuracy of minority class samples, thereby enhancing the F1 score. Furthermore, the decision boundary that maximizes accuracy on the noisy data coincides with the optimal F1 decision boundary on the original data when $\frac{\mathcal{F}1(x^*)}{2 - \mathcal{F}1(x^*)} = 1 - 2\rho(x^*)$.

Similar as in Section 3.2, consider the classifier $\hat{Y}^* = \mathbb{I}(\omega^T(X - x_0^*) > 0)$ for some $\omega \in \mathbb{R}^d$ and $x_0^* \in \mathcal{X}$, trained on the noisy data. Define the corresponding population F1 score as $\mathcal{F}1^*(x_0^*) = \frac{2\pi_1^* \mathcal{P}_1^*(x_0^*)}{\pi_1^* \mathcal{P}_1^*(x_0^*) + \pi_0^* \mathcal{P}_0^*(x_0^*) + \pi_1^*}$, where $\mathcal{P}_1^*(x_0^*) = \Pr(\omega^T(X - x_0^*) > 0 \mid Y^* = 1)$ and $\mathcal{P}_0^*(x_0^*) = \Pr(\omega^T(X - x_0^*) > 0 \mid Y^* = 0)$, $\pi_1^* = \Pr(Y^* = 1)$ and $\pi_0^* = \Pr(Y^* = 0) = 1 - \pi_1^*$. The decision boundary that maximizes $\mathcal{F}1^*(x_0^*)$ based on relabeled sample (X, Y^*) is

$$S^{\mathrm{F}1*} = \left\{ x_0^* \in \mathcal{X} : \frac{\mathcal{P}_1^*(x_0^*)}{\mathcal{P}_0^*(x_0^*)} = \frac{\mathcal{F}1^*(x_0^*)}{2 - \mathcal{F}1^*(x_0^*)} \frac{\pi_0^*}{\pi_1^*} \right\}.$$

Under the relabeled data, it is expected that $\mathcal{P}_1^*(x_0^*)/\mathcal{P}_0^*(x_0^*)$ and π_1^*/π_0^* will increase compared to $P_1(x^*)/P_0(x^*)$ and π_1/π_0. Therefore, compared to the original decision boundary $S^{\mathrm{F}1}$ that maximizes $\mathcal{F}1(x_0)$, we expect an increase in $\mathcal{F}1^*(x_0^*)$, the maximum F1 score under the noisy data.

Algorithm 1 Flip labels in binary classification with noise model $\rho(x)$

Input: Feature X and labels Y, Classifier C_f
Parameters: Threshold t_{flip}
$\text{Ind}_{\text{MA}} \leftarrow \texttt{index}(Y=0), \hat{\eta}, \mathcal{Z}, \rho \leftarrow \texttt{zeroVector}(size=N)$
for $i \in 1 \rightarrow \mathit{length}(Y)$ **do**
  $\hat{\eta}[i] \leftarrow C_f(X[i])$
end
$\mu \leftarrow \texttt{mean}(\hat{\eta}[\text{Ind}_{\text{MA}}]), \quad \sigma \leftarrow \texttt{std}(\hat{\eta}[\text{Ind}_{\text{MA}}])$
for each i_{MA} in Ind_{MA} **do**
  $\mathcal{Z}[i_{\text{MA}}] \leftarrow \frac{\hat{\eta}[i_{\text{MA}}]-\mu}{\sigma}$
  $\rho[i_{\text{MA}}] \leftarrow max(\texttt{tanh}(\mathcal{Z}[i_{\text{MA}}]-t_{flip}), 0)$
  $\text{U} \leftarrow \text{Bernoulli}(\rho[i_{\text{MA}}])$
  if $\text{U} == 1$ **then**
    $Y[i_{\text{MA}}] \leftarrow 1$
  end
end
Return: Y

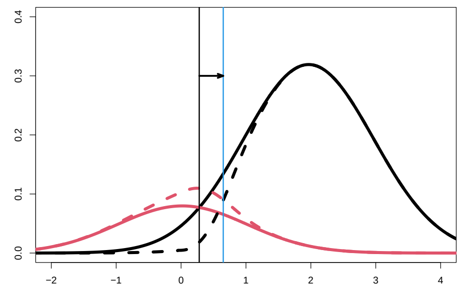

Figure 3: Asymmetric label noise shifts the biased decision boundary towards the majority class region, where the dashed lines are sample distributional densities after label flipping. The majority class samples deep into the minority region have the higher flip-rates $\rho(x)$.

In summary, with an asymmetric instance-dependent noise model, the artificial label noise can correct the biased decision boundaries caused by class imbalance, improving the classification accuracy of minority class samples. The F1 score is expected to increase under the noisy data, demonstrating the effectiveness of the asymmetric label noise model in imbalanced classification.

4.2. Constructing noise model in binary classification

Estimating the flip-rate $\rho(x)$, which is proportional to $\eta(x)$ in binary classification, is crucial. We propose utilizing the posterior probabilities $\hat{\eta}(x)$ obtained from an arbitrary classifier trained on imbalanced data to approximate $\eta(x)$, thereby constructing the label noise model $\rho(x)$. The noise model is constructed using Algorithm 1:

Step 1. Train a classifier C_f on the original imbalanced data and obtain the posterior probabilities $\hat{\eta}[i] = C_f(X[i])$. Although $\hat{\eta}[i]$ may be biased or underestimating $\eta(x)$, the majority class samples with features similar to minority class samples still tend to exhibit relatively higher posterior probabilities of being classified into minority classes. As a result, these samples are expected to have relatively higher probabilities of being relabeled as the minority class.

Step 2. Employ z-score standardization on $\hat{\eta}[i_{\text{MA}}]$ to get $\mathcal{Z}[i_{\text{MA}}]$, where i_{MA} is the index of each majority class sample. This magnifies the differentiation in the posterior probabilities of majority class samples. The deviation level, measured by $\mathcal{Z}[i_{\text{MA}}]$, ranks majority class samples in proportion to their similarity to the minority class samples.

Step 3. Rescale $\mathcal{Z}[i_{\text{MA}}]$ to $[0,1]$ by calculating $\rho[i_{\text{MA}}] = \texttt{max}(\texttt{tanh}(\mathcal{Z}[i_{\text{MA}}]-t_{flip}), 0)$, where the threshold t_{flip} is a tunable parameter for selecting appropriate samples with high similarities to minority class features. Notably, $\texttt{tanh}(\mathcal{Z}[i_{\text{MA}}]-t_{flip}) > 0$ when $\mathcal{Z}[i_{\text{MA}}] > t_{flip}$, which zeros the flip rates of majority class samples below t_{flip}.

Step 4. Flip majority class samples into minority class according to their flip rate $\rho[i_{\text{MA}}]$,

Empirically, t_{flip} can be selected by cross-validation. See Section 5 and Appendix for more discussions.

4.3. Extend to multi-class classification

Unlike binary classification tasks that contain only one minority class, multi-class data may include multiple minority class samples. To make LNR adopt the various imbalance ratios between classes, we weigh the flip rate of being flipped into different classes by the class prior weight vector $\theta_{\mathcal{C}}$, where $\mathcal{C}$ is the class vector. These weights are calculated based on the sample sizes $N_{\mathcal{C}}$, and $\texttt{max}(\theta_{\mathcal{C}} - \theta_{\mathcal{C}}[y], 0)$ guarantees label flipping is only proceeded from majority class to minority class and preventing label flipping between classes with the same class prior. The label-flipping procedure for multi-class scenarios is detailed in Algorithm 2.

Due to that more complex neural networks are typically used in multi-class image classification tasks, training a separate flipping rate estimator is costly, unlike in binary classification scenarios. As our method allows for using any classifier as the flipping rate estimator, we directly utilize the model itself to calculate the posterior probabilities with $\texttt{softmax}(fc(w^t; X, Y))$ during training, where $fc(w^t; X, Y)$ is the output of the last fully-connected layer of model w^t at epoch t. Similar to the Deferred Re-Weighting (DRW) approach (Cao et al., 2019), we postpone

Algorithm 2 Constructing label noises during training at round t

Input: Feature X and labels Y, and the model w^t at current epoch t
Parameters: Flipping threshold t_{flip}, Deferred epochs T_D
$\mathrm{Q} \leftarrow \texttt{softmax}(fc(w^t; X, Y))$ where $fc(w^t; \cdot, \cdot)$ is the last fully-connected layer output of model w^t
$\theta_{\mathcal{C}} \leftarrow 1 - \textbf{minMax}(N_{\mathcal{C}})$ where $N_{\mathcal{C}}$ counts the samples of each class
$\mu \leftarrow \texttt{mean}(\mathrm{Q})$, $\gamma \leftarrow \texttt{std}(\mathrm{Q})$
for $(x, y^t) \in (X, Y)$ **do**
  Calculate Z-score for sample x: $\mathcal{Z}_x \leftarrow \frac{\mathrm{Q}[x]-\mu}{\gamma}$
  Get the flipping strength for class $c \in \mathcal{C}$: $\theta_{c=y} \leftarrow \texttt{max}(\theta_{\mathcal{C}} - \theta_{\mathcal{C}}[y], 0)$
  Calculate the class-wize flip-rate for sample x: $\mathcal{F}_x \leftarrow \texttt{max}(\texttt{tanh}(\mathcal{Z}_x - t_{flip}), 0) \times \theta_{c=y}$
  $\mathcal{U} \leftarrow \mathrm{Bernoulli}(\mathcal{F}_x)$ `# generated by independent Bernoulli distribution with` $\mathcal{F}_x$.
  if $\mathcal{U}$ *contains 1 and* $t > T_D$ **then**
    $y^t \leftarrow \mathcal{C}[\texttt{indexOf}(\texttt{max}(\mathcal{F}_x\,[\mathcal{U} == 1]))]$ where $\mathcal{C}$ is the class vector.
  end
  Update the model w^t with (x, y^t)
end

the introduction of label noise until the model has converged (after T_D epochs) in the fine-tuning stage leveraging possible influence on the feature extraction process.

It is important to note that the posterior probabilities produced by a multi-class model form a $C \times 1$ vector where C is the number of classes. A majority class sample has $C - 1$ posterior probabilities corresponding to being classified as other classes, resulting in $C - 1$ distinct flipping rates. In the case of majority class samples exhibiting similar features to multiple minority classes, resulting in multiple high flip rates, we flip such majority samples into the minority class having the highest flip rate. Random flipping is employed in the event of a tie on flip rates.

5. Experimental Evaluations

Datasets. *Imbalanced Binary classification:* We evaluated LNR on 32 datasets from the KEEL repository (Derrac et al., 2015), featuring a wide range of imbalance ratios from 1.82 to 49.6. Summary statistics of these datasets can be found in Table 7 in the Appendix. The criteria for selecting these 32 datasets are detailed in Appendix C.5. *Imbalanced Multi-class classification:* We conducted experiments on two multi-class image datasets: CIFAR-10 and CIFAR-100. As the datasets are initially balanced, we artificially create step-wise and long-tailed imbalanced versions of these datasets with the imbalance ratio of $N_{max}/N_{min} = 100$, where N_{max} and N_{min} are the sample size of largest class and smallest class. Step-wise imbalance was created by removing 99% of samples from half of the classes, while long-tailed imbalance was generated by exponentially reducing sample sizes per class to satisfy the imbalance ratio. Appendix C.5 provides further details. Additional experimental results on synthetic data are in Appendix C.5.

Classifiers. As data-level methods can be coupled with many classifiers, we run the experiments with three commonly used classifiers on KEEL datasets: k-nearest neighbor (KNN) (Cover & Hart, 1967), CART (Quinlan, 1986), and multi-layer perceptron (MLP) (Rumelhart & Williams, 1986). For multi-class datasets, the Resnet-32 is used for all methods. The classifier parameters and implement details are in Appendix C.2.

Baseline and prior methods. For binary classification, the *baseline* trains the classifier with the original imbalanced data. We compare our method, *LNR*, with well-known resampling method, including over-sampling methods: *SMOTE* (Chawla et al., 2002), *ADASYN* (He et al., 2008), and *Borderline* (Han et al., 2005); and undersampling methods: *Random-Under-Sampling (RUS)*, *OSS* (Kubat & Matwin, 2000), and *CC* (ClusterCentroids) (Lin et al., 2017). *LNR* adapts the final layer of the MLP classifier to include a soft-max function as the flip-rate estimator C_f, trained on the original data for KEEL datasets.

For image classification tasks, the baseline is the algorithm-level approach *LDAM-DRW* (Cao et al., 2019), and we compared our method with the data-level method *RSG* (Wang et al., 2021a) integrating with the baseline. We also show the improvement of our approach combined with a more recent algorithm-level approach *GCL* (Li et al., 2022c). On long-tailed CIFAR-10/100, we also compared our method with mixup-based methods *ReMix* (Chou et al., 2020) and the latest SOTA *SelMix* (Ramasubramanian et al., 2024) on top of the algorithm-level SOTA *MiSLAS* (Zhong et al., 2021). As SelMix relies on a balanced auxiliary dataset D_{val}, we denote its original implementation as *10k* ($|D_{\mathrm{val}}| = 10000$). We also compare with a smaller size of $|D_{\mathrm{val}}| = 1000$, denoted as (*1k*), and an imbalanced (*imb*) validation dataset.

Hyperparameters for all methods were selected via grid search within the ranges specified in Appendix C.2.

Evaluation metrics. To ensure a comprehensive evaluation, we report multiple widely used metrics. For step-wise imbalanced multi-class datasets, we report the average minority class accuracy $\mathrm{Acc}_{\mathrm{MI}}$ and the overall accuracy $\mathrm{Acc}_{\mathrm{overall}}$, as we expect to obtain higher recall on minority classes without sacrificing the overall accuracy. For long-tailed datasets, we compare their average accuracy of **Many-shot**, **Medium-shot**, and **Few-shot** groups of classes. For the binary classification on KEEL, we used **F1 score**, **G-mean**, and **AUC**. The F1 score and G-mean focus on the performance of classifying minority class samples, while AUC is more conservative, as it is sensitive to the error rate of the majority class samples. Appendix C.7 shows the metrics definition and detailed evaluation settings.

Results on step-wise imbalanced data. Table 1 reports the comparison of our method with the SOTA data-level method RSG and the SOTA algorithm-level method GCL on CIFAR-10/100 datasets. Without sacrificing the overall accuracy, our method outperforms the previous data-level SOTA (RSG) by 8.04% and 4.2% and the previous algorithm-level SOTA (GCL) by 15.44% and 21% in terms of the accuracy of minority classes on stepwise CIFAR-10 and CIFAR-100 respectively. Results also demonstrate the significant improvement achieved by combining LNR with algorithm-level methods of LDAM-DRW and GCL.

Table 1: Comparision on Step-wise CIFAR-10/100 Datasets in the format of (mean % ±std).

	Step-wise Cifar-10		**Step-wise Cifar-100**	
	$\mathrm{Acc}_{\mathrm{MI}}$	$\mathrm{Acc}_{\mathrm{overall}}$	$\mathrm{Acc}_{\mathrm{MI}}$	$\mathrm{Acc}_{\mathrm{overall}}$
LDAM	66.41±0.2	77.47±0.06	19.80±0.02	45.23±0.03
LDAM+RSG	67.02±0.07	77.74±0.08	21.67±0.04	45.51±0.02
LDAM+LNR	**75.06±0.09**	**78.12±0.03**	**25.84±0.06**	**45.63±0.02**
GCL	56.78±0.08	74.80±0.04	5.48 ±0.03	43.87±0.07
GCL+LNR	**72.22±0.05**	**80.8±0.02**	**26.48±0.03**	**46.20±0.03**

Results on Long-tail Cifar-10/100. Due to the scarcity of tail classes, there is often heightened interest in their classification accuracy, commonly termed few-shot accuracy. As shown in Table 2, our method achieves state-of-the-art performance on both CIFAR10-LT and CIFAR100-LT under an extreme imbalance ratio of $\mathrm{IR} = 100$. By integrating with algorithm-level methods such as LDAM, GCL, and MiSLAS, LNR significantly improves tail-class performance without compromising overall accuracy. Crucially, LNR eliminates the dependency on balanced validation data–a key advantage over SelMix, which requires 10k balanced auxiliary samples (equivalent to $20\times$ the tail-class training data) yet suffers significant performance degradation with smaller or imbalanced validation sets. Notably, LNR achieves SOTA performance on CIFAR-10/100-LT by injecting only 44 and 65 instances of label noise into the original data, respectively, demonstrating the effectiveness of our noise model.

Table 2: Comparision on Long-tailed CIFAR-10/100 Datasets in the format of (mean % ±std).

	Long-tailed Cifar-10			
	Many-shot	**Medium-shot**	**Few-shot**	**Overall**
LDAM	**82.62±0.06**	76.12±0.1	75.01±0.1	78.39±0.03
LDAM+RSG	81.56±0.15	**77.03±0.1**	77.30±0.1	78.93±0.02
LDAM+LNR	81.17±0.08	76.42±0.01	**79.83±0.1**	**79.34±0.01**
GCL	**88.60±0.04**	**79.57±0.01**	70.08±0.2	80.55±0.03
GCL+LNR	88.20±0.04	79.50±0.07	**77.60±0.2**	**82.41±0.03**
MiSLAS	**91.00±0.14**	80.17±0.22	75.72±0.19	82.10±0.12
MiSLAS+ReMix	90.04±0.20	79.82±0.16	79.78±0.20	82.92±0.10
MiSLAS+SelMix(10k)	86.81±0.22	80.50±0.17	83.52±0.21	83.29±0.07
MiSLAS+SelMix(1k)	81.61±0.14	79.89±0.13	**87.60±0.20**	82.72±0.22
MiSLAS+SelMix(imb)	82.21±0.13	81.44±0.11	81.9±0.21	81.8 ±0.09
MiSLAS+LNR	84.62±0.22	**80.90±0.22**	86.07±0.19	**83.56**±0.08
	Long-tailed Cifar-100			
	Many-shot	**Medium-shot**	**Few-shot**	**Overall**
LDAM	**62.21±0.05**	43.28±0.08	20.83±0.03	42.98±0.03
LDAM+RSG	60.46±0.05	**43.88±0.1**	22.57±0.09	43.08±0.07
LDAM+LNR	61.04±0.03	43.36±0.02	**24.11±0.04**	**43.58±0.02**
GCL	**67.16±0.03**	46.63±0.06	13.57±0.06	43.90±0.03
GCL+LNR	57.11±0.07	**51.38±0.07**	**25.02±0.09**	**45.48±0.05**
MiSLAS	**62.05±0.09**	48.42±0.11	26.07±0.12	46.85±0.09
MiSLAS+ReMix	59.06±0.21	49.22±0.09	27.93±0.10	46.59±0.15
MiSLAS+SelMix(10k)	60.93±0.12	**52.06±0.17**	25.10±0.13	47.43±0.10
MiSLAS+SelMix(1k)	61.27±0.08	50.82±0.18	21.34±0.12	46.04 ±0.11
MiSLAS+SelMix(imb)	56.66±0.12	51.17±0.06	25.31±0.21	45.65 ±0.23
MiSLAS+LNR	56.26±0.24	51.46±0.22	**35.34±0.21**	**48.52** ±0.12

Table 3: Expected Calibration Error (ECE).

ECE	MiSLAS	+ReMix	+SelMix	+SelMix(imb)	+LNR
CIFAR-10	3.70	19.62	**2.75**	6.36	5.16
CIFAR-100	5.43	18.28	**1.32**	3.01	9.55

Model Calibration. MiSLAS (Zhong et al., 2021) empirically observed that applying mixup-based methods like ReMix during the fine-tuning stage severely degrades model calibration (measured by ECE). As shown in Table 3, ReMix significantly increases ECE. In contrast, although LNR also slightly affects calibration accuracy, these minor degradations are acceptable given its substantial improvements in classification performance.

SelMix benefits from calibration using a balanced auxiliary dataset, achieving lower ECE. However, when the auxiliary dataset becomes imbalanced, SelMix's calibration improvement weakens, resulting in higher ECE than LNR on CIFAR-10. Crucially, LNR requires no auxiliary dataset. By flipping only a small number of labels while preserving original data features (no feature modification), it maximizes overall classifier performance, especially for minority classes, while maintaining ECE within acceptable bounds. This highlights LNR's practical superiority in balancing accuracy and reliability under real-world data constraints.

Model fairness. To demonstrate model fairness improvements brought by LNR, we compare the confusion matrices

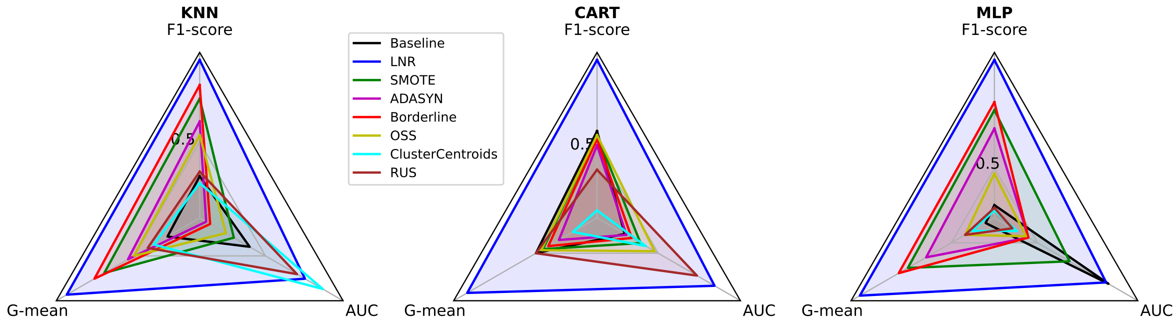

Figure 4: Relative ranking of methods from 1 (the best) to 0 (the lowest) on 32 KEEL datasets.

of GCL and GCL+LNR on long-tailed CIFAR10 in Table 3. LNR introduced 94 label noises, including 41 samples relabeled as tail class "8: ship", 44 samples relabeled as tail class "9: truck" from head class "0: airplane", and 6 samples relabeled as tail class "9: truck" from head class "1: automobile". Despite the extreme imbalance ratio between head classes and the tail class "7: horse", no samples were flipped into class "7: horse", as LNR flips are based on feature similarity, making these flips controlled and self-limiting. The bold diagonal numbers demonstrate that LNR achieves an effective trade-off between the classification performance of the head class (yellow) and the tail class (green). While there is a slight reduction in head classes (16 fewer true positives), LNR leads to a substantial improvement in the performance of tail classes (204 more true positives). Simultaneously, LNR significantly reduces tail-to-head misclassifications (blue) with minor increased head-to-tail misclassifications (red), preserving the model fairness across different classes.

	0	1	2	3	4	5	6	7	8	9
0	**-26**	+2	-4	0	+1	-2	0	-1	**+13**	**+16**
1	**1**	**-4**	0	-1	+1	0	0	0	**0**	**+4**
2	5	+1	**-4**	-2	0	-7	+1	+3	-1	+3
3	-2	-1	+3	**+18**	-4	-13	-5	+2	0	+5
4	0	0	-2	-3	**+3**	-5	0	+5	+1	+1
5	2	0	-1	-3	0	**-1**	+1	+2	0	+2
6	1	+2	-2	+6	-1	-5	**-4**	+2	-1	+1
7	-5	0	+3	-20	-1	-8	+4	**+22**	+1	+5
8	**-91**	-6	+2	-2	-1	-1	-2	0	**+80**	+20
9	**-42**	**-48**	-3	-5	+1	-2	-3	-2	+3	**+102**

Table 4: Confusion matrix comparison of GCL and LNR. The signed values denote the changes made by LNR.

By selectively flipping the labels of samples near the decision boundary that share similar features with minority class samples, LNR minimizes the data editing and achieves a more efficient correction of the biased decision boundary, which offers us significant improvements in the accuracy of minority classes without sacrificing the overall accuracy.

Results on KEEL results. The relative rankings shown in Figure 4 demonstrate that our method achieved the highest average performance across 32 datasets for all three classifiers in both F1 score and G-mean. In addition to these rankings, we calculated the Pearson correlation coefficients between the relative performance differences of our method and other methods, and the data distribution characteristics. The numeric results are detailed in Table 11 in Appendix C.7. Our method demonstrated superior F1 score and G-mean performance on data with higher class overlap, attributed to reduced class overlap through label flipping at decision boundaries. In highly imbalanced data settings, oversampling methods require synthesizing oversized samples to balance the data, which exacerbates generative errors and increases the error rate for majority class samples, thereby hampering AUC performance. On the contrary, LNR does not involve adding or removing samples, significantly enhancing F1 score and G-mean scores without compromising AUC performance.

6. Conclusion

In this paper, we theoretically analyze the impact mechanisms of imbalanced data on classifiers. By investigating the influence of label noise on the data, we propose a novel method, LNR, of artificially introducing label noise to enhance the performance of imbalanced learning. LNR introduces a novel asymmetric label-noise model that strategically flips labels to adjust decision boundaries in imbalanced learning while avoiding information loss or generative errors inherent in traditional resampling and augmentation methods. LNR not only demonstrates comprehensive superiority on synthetic and KEEL datasets but also achieves state-of-the-art performance on step-wise and long-tailed imbalanced image classification benchmarks. In addition, LNR can integrate seamlessly with any classifiers and other algorithm-level methods for imbalanced learning.

Impact Statement

This paper presents work whose goal is to advance the field of Machine Learning. There are many potential societal consequences of our work, none of which we feel must be specifically highlighted here.

Acknowledgements

FL is supported by the Australian Research Council (ARC) (Grant No. DE240101089, LP240100101, DP230101540) and the NSF&CSIRO Responsible AI program (Grant No. 2303037). MG was supported by ARC DE210101624, ARC DP240102088, and WIS-MBZUAI 142571. GW was supported by the National Natural Science Foundation of China (Grant No. 12471255), the Natural Science Foundation of Shanghai (Grant No. 23ZR1419400), and the Fundamental Research Funds for the Central Universities (Grant No. 63253110). LP is supported by ARC (Grant No. LP240100101).

References

Ahfock, D. and McLachlan, G. Harmless label noise and informative soft-labels in supervised classification. *Computational Statistics & Data Analysis*, 161:107253, 2021.

Azaria, A., Richardson, A., Kraus, S., and Subrahmanian, V. S. Behavioral analysis of insider threat: A survey and bootstrapped prediction in imbalanced data. *IEEE Transactions on Computational Social Systems*, 1(2):135–155, 2014.

Cannings, T. I., Fan, Y., and Samworth, R. J. Classification with imperfect training labels. *Biometrika*, 107(2):311–330, 2020.

Cao, K., Wei, C., Gaidon, A., Arechiga, N., and Ma, T. Learning imbalanced datasets with label-distribution-aware margin loss. volume 32, 2019.

Chawla, N., Bowyer, K., Hall, L., and Kegelmeyer, W. P. Smote: synthetic minority over-sampling technique. *Journal of artificial intelligence research*, 16:321–357, 2002.

Chawla, N. V., Japkowicz, N., and Kotcz, A. Special issue on learning from imbalanced data sets. *ACM SIGKDD explorations newsletter*, 6(1):1–6, 2004.

Chou, H.-P., Chang, S.-C., Pan, J.-Y., Wei, W., and Juan, D.-C. Remix: rebalanced mixup. In *European conference on computer vision*, pp. 95–110. Springer, 2020.

Cover, T. and Hart, P. Nearest neighbor pattern classification. *IEEE transactions on information theory*, 13(1):21–27, 1967.

Derrac, J., Garcia, S., Sanchez, L., and Herrera, F. Keel data-mining software tool: Data set repository, integration of algorithms and experimental analysis framework. *J. Mult. Valued Log. Soft Comput*, 17:255–287, 2015.

Fotouhi, S., Asadi, S., and Kattan, M. A comprehensive data level analysis for cancer diagnosis on imbalanced data. *Journal of biomedical informatics*, 90:103089, 2019.

Frénay, B. and Verleysen, M. Classification in the presence of label noise: a survey. *IEEE transactions on neural networks and learning systems*, 25(5):845–869, 2013.

Goldberger, J. and Ben-Reuven, E. Training deep neural-networks using a noise adaptation layer. *International conference on learning representations*, 2022.

Han, H., Wang, W.-Y., and Mao, B.-H. Borderline-smote: a new over-sampling method in imbalanced data sets learning. *International conference on intelligent computing*, 2005.

He, H. and Garcia, E. Learning from imbalanced data. *IEEE Transactions on knowledge and data engineering*, 21(9): 1263–1284, 2009.

He, H., Bai, Y., Garcia, E., and Li, S. Adasyn: Adaptive synthetic sampling approach for imbalanced learning. *2008 IEEE international joint conference on neural networks*, 2008.

Hou, C., Zhang, J., Wang, H., and Zhou, T. Subclass-balancing contrastive learning for long-tailed recognition. In *Proceedings of the IEEE/CVF international conference on computer vision*, pp. 5395–5407, 2023.

Kang, B., Xie, S., Rohrbach, M., Yan, Z., Gordo, A., Feng, J., and Kalantidis, Y. Decoupling representation and classifier for long-tailed recognition. *arXiv preprint arXiv:1910.09217*, 2019.

Kaur, H., Pannu, H. S., and Malhi, A. K. A systematic review on imbalanced data challenges in machine learning: Applications and solutions. *ACM Computing Surveys (CSUR)*, 52(4):1–36, 2019.

Krawczyk, B. Learning from imbalanced data: open challenges and future directions. *Progress in Artificial Intelligence*, 5(4):221–232, 2016.

Kubat, M. and Matwin, S. Addressing the curse of imbalanced training sets: One-sided selection. *Fourteenth International Conference on Machine Learning*, 2000.

Li, B., Han, Z., Li, H., Fu, H., and Zhang, C. Trustworthy long-tailed classification. In *Proceedings of the IEEE/CVF Conference on Computer Vision and Pattern Recognition*, pp. 6970–6979, 2022a.

Li, J., Tan, Z., Wan, J., Lei, Z., and Guo, G. Nested collaborative learning for long-tailed visual recognition. pp. 6949–6958, 2022b.

Li, M., Cheung, Y.-m., and Lu, Y. Long-tailed visual recognition via gaussian clouded logit adjustment. In *Proceedings of the IEEE/CVF Conference on Computer Vision and Pattern Recognition (CVPR)*, pp. 6929–6938, June 2022c.

Li, T., Cao, P., Yuan, Y., Fan, L., Yang, Y., Feris, R. S., Indyk, P., and Katabi, D. Targeted supervised contrastive learning for long-tailed recognition. In *Proceedings of the IEEE/CVF conference on computer vision and pattern recognition*, pp. 6918–6928, 2022d.

Lin, W.-C., Tsai, C.-F., Hu, Y.-H., and Jhang, J.-S. Clustering-based undersampling in class-imbalanced data. *Information Sciences*, 409-410:17–26, 2017. ISSN 0020-0255.

Liu, T. and Tao, D. Classification with noisy labels by importance reweighting. *IEEE Transactions on pattern analysis and machine intelligence*, 38(3):447–461, 2015.

Napierala, K. and Stefanowski, J. Types of minority class examples and their influence on learning classifiers from imbalanced data. *Journal of Intelligent Information Systems*, 46:563–597, 2016.

Patrini, G., Rozza, A., Krishna Menon, A., Nock, R., and Qu, L. Making deep neural networks robust to label noise: A loss correction approach. *Proceedings of the IEEE conference on computer vision and pattern recognition*, 2017.

Phua, C., Alahakoon, D., and Lee, V. Minority report in fraud detection: classification of skewed data. *ACM SIGKDD Explorations Newsletter*, 6(1):50–59, 2004. ISSN 1931-0145.

Quinlan, R. Induction of decision trees. *Machine learning*, 1:81–106, 1986.

Ramasubramanian, S., Rangwani, H., Takemori, S., Samanta, K., Umeda, Y., and Radhakrishnan, V. B. Selective mixup fine-tuning for optimizing non-decomposable metrics. In *The Twelfth International Conference on Learning Representations*, 2024.

Rumelhart, David, H. G. and Williams, R. Learning representations by back-propagating errors. *Nature*, 323: 533–536, 1986.

Saerens, M., Latinne, P., and Decaestecker, C. Adjusting the outputs of a classifier to new a priori probabilities: a simple procedure. *Neural computation*, 14(1):21–41, 2002.

Samuel, D. and Chechik, G. Distributional robustness loss for long-tail learning. In *Proceedings of the IEEE/CVF international conference on computer vision*, pp. 9495–9504, 2021.

Schwartz, E., Karlinsky, L., Shtok, J., Harary, S., Marder, M., Kumar, A., Feris, R., Giryes, R., and Bronstein, A. Delta-encoder: an effective sample synthesis method for few-shot object recognition. *Advances in neural information processing systems*, 31, 2018.

Song, H., Kim, M., Park, D., Shin, Y., and Lee, J.-G. Learning from noisy labels with deep neural networks: A survey. *IEEE Transactions on Neural Networks and Learning Systems*, 34(11):8135–8153, 2022.

Tomek, I. Two modifications of cnn. *IEEE Transactions on Systems, Man, and Cybernetics*, SMC-6(11):769–772, 1976.

Wang, J., Lukasiewicz, T., Hu, X., Cai, J., and Xu, Z. Rsg: A simple but effective module for learning imbalanced datasets. pp. 3784–3793, June 2021a.

Wang, X., Lyu, Y., and Jing, L. Deep generative model for robust imbalance classification. June 2020.

Wang, X., Lian, L., Miao, Z., Liu, Z., and Yu, S. Long-tailed recognition by routing diverse distribution-aware experts. In *International Conference on Learning Representations*, 2021b.

Wilson, R. and Martinez, T. Reduction techniques for instance-based learning algorithms. *Machine learning*, 38:257–286, 2000.

Xiao, T., Xia, T., Yang, Y., Huang, C., and Wang, X. Learning from massive noisy labeled data for image classification. *Proceedings of the IEEE conference on computer vision and pattern recognition*, 2015.

Xu, H., Liu, X., Li, Y., Jain, A., and Tang, J. To be robust or to be fair: Towards fairness in adversarial training. In *International conference on machine learning*, pp. 11492–11501. PMLR, 2021.

Zhang, H., Cisse, M., Dauphin, Y. N., and Lopez-Paz, D. mixup: Beyond empirical risk minimization. *arXiv preprint arXiv:1710.09412*, 2017.

Zhang, Y., Hooi, B., Hong, L., and Feng, J. Self-supervised aggregation of diverse experts for test-agnostic long-tailed recognition. *Advances in neural information processing systems*, 35:34077–34090, 2022.

Zhong, Z., Cui, J., Liu, S., and Jia, J. Improving calibration for long-tailed recognition. In *Proceedings of the IEEE/CVF conference on computer vision and pattern recognition*, pp. 16489–16498, 2021.

Zhu, J., Wang, Z., Chen, J., Chen, Y.-P. P., and Jiang, Y.-G. Balanced contrastive learning for long-tailed visual recognition. In *Proceedings of the IEEE/CVF conference on computer vision and pattern recognition*, pp. 6908–6917, 2022.

Zhu, X., Wu, X., and Chen, Q. Eliminating class noise in large datasets. *Proceedings of the 20th International Conference on Machine Learning*, 2003.

A. Proofs

A.1. Proof of Lemma 1

Proof. By Bayes theorem,

$$\eta(x) = \Pr(Y = 1 \mid X = x) = \frac{\pi_1 P_1(x)}{\pi_1 P_1(x) + \pi_0 P_0(x)}.$$

Thus, $\eta(x) = 0.5$ is equivalent to $\frac{P_1(x)}{P_0(x)} = \frac{\pi_0}{\pi_1}$. □

For Gaussian data with $P_0 \sim N(\mu_0, \Sigma)$ and $P_1 \sim N(\mu_1, \Sigma)$, $\frac{P_1(x)}{P_0(x)} = \frac{\pi_0}{\pi_1}$ is equivalent to

$$\frac{\exp\left\{-\frac{1}{2}(x-\mu_1)^T\Sigma^{-1}(x-\mu_1)\right\}}{\exp\left\{-\frac{1}{2}(x-\mu_0)^T\Sigma^{-1}(x-\mu_0)\right\}} = \frac{\pi_0}{\pi_1},$$

and this can be simplified to

$$\omega^T x + \beta = \ln\left(\frac{\pi_0}{\pi_1}\right)$$

with $\omega = \Sigma^{-1}(\mu_1 - \mu_0)$ and $\beta = \frac{1}{2}\mu_0^T\Sigma^{-1}\mu_0 - \frac{1}{2}\mu_1^T\Sigma^{-1}\mu_1$.

A.2. Proof of Lemma 2

Proof. The population version of the F1 score is defined as

$$\mathcal{F}1(x_0) = \frac{2\pi_1\mathcal{P}_1(x_0)}{\pi_1\mathcal{P}_1(x_0) + \pi_0\mathcal{P}_0(x_0) + \pi_1}. \tag{3}$$

where $\mathcal{P}_1(x_0) = \Pr(\omega^T(X - x_0) > 0 \mid Y = 1)$, and $\mathcal{P}_0(x_0) = \Pr(\omega^T(X - x_0) > 0 \mid Y = 0)$.

Here, we denote the numerator as $A = 2\pi_1\mathcal{P}_1(x_0)$ and the denominator as $B = \pi_1\mathcal{P}_1(x_0) + \pi_0\mathcal{P}_0(x_0) + \pi_1$. The $\mathrm{argmax}_{x_0\in\mathcal{X}}\mathcal{F}1(x_0)$ can be found by letting $\frac{\partial\mathcal{F}1(x_0)}{\partial x_0} = 0$, that is,

$$\frac{\partial\mathcal{F}1(x_0)}{\partial x_0} = \frac{A'B - B'A}{B^2} = 0$$

where $A' = \frac{\partial A}{\partial x_0}$ and $B' = \frac{\partial B}{\partial x_0}$. As $B > 0$, we have

$$A'B = B'A. \tag{4}$$

Assume exchangeability of integration and differentiation, the Leibniz integral rule implies $\partial\mathcal{P}_1(x_0)/\partial x_0 = -P_1(x_0)\omega$ and $\partial\mathcal{P}_0(x_0)/\partial x_0 = -P_0(x_0)\omega$. By substituting

$$A' = -2\pi_1 P_1(x_0)\omega,\ B' = -\pi_1 P_1(x_0)\omega - \pi_0 P_0(x_0)\omega$$

into (4), we obtain that

$$-2\pi_1 P_1(x_0)\left(\pi_1\mathcal{P}_1(x_0) + \pi_0\mathcal{P}_0(x_0) + \pi_1\right)\omega = 2\pi_1\mathcal{P}_1(x_0)\left(-\pi_1 P_1(x_0)\omega - \pi_0 P_0(x_0)\omega\right),$$

which is equivalent to

$$\frac{2\pi_1 P_1(x_0)}{\pi_1 P_1(x_0) + \pi_0 P_0(x_0)} = \mathcal{F}1(x_0). \tag{5}$$

Rearranging the equation results in

$$\frac{P_1(x_0)}{P_0(x_0)} = \frac{\mathcal{F}1(x_0)}{2 - \mathcal{F}1(x_0)}\frac{\pi_0}{\pi_1},$$

which indicates that the decision boundary that maximizes the population F1 score is of the form

$$S^{\mathrm{F1}} = \left\{x_0 \in \mathcal{X} : \frac{P_1(x_0)}{P_0(x_0)} = \frac{\mathcal{F}1(x_0)}{2 - \mathcal{F}1(x_0)}\frac{\pi_0}{\pi_1}\right\}.$$

□

A.3. Proof of Lemma 4.1

Proof. First,

$$\begin{aligned}\eta^*(x) &= \Pr(Y^*=1 \mid X=x, Y=1)\Pr(Y=1 \mid X=x) \\ &\quad + \Pr(Y^*=1 \mid X=x, Y=0)\Pr(Y=0 \mid X=x) \\ &= \eta(x) + \rho(x)[1-\eta(x)] \\ &= \eta(x)[1-\rho(x)] + \rho(x).\end{aligned}$$

As x^* satisfies $\eta^*(x^*) = 0.5$ with the constrain of $\rho(\hat{x}^*) < 0.5$, we have $\eta(x^*)[1-\rho(x^*)] + \rho(x^*) = 0.5$, which is equivalent to

$$\frac{\pi_1 P_1(x^*)}{\pi_1 P_1(x^*) + \pi_0 P_0(x^*)}[1-\rho(x^*)] + \rho(x^*) = \frac{1}{2}.$$

It follows that

$$\frac{P_1(x^*)}{P_0(x^*)} = [1-2\rho(x^*)]\frac{\pi_0}{\pi_1}.$$

Thus, the optimal Bayesian decision boundary that maximizes the accuracy on the noisy dataset (X, Y^*) is defined as:

$$S^* = \left\{x^* \in \mathcal{X} : \frac{P_1(x^*)}{P_0(x^*)} = [1-2\rho(x^*)]\frac{\pi_0}{\pi_1}\right\}.$$

□

For one-dimensional normal distributed data with $P_1 \sim N(\mu_1, \sigma^2)$ and $P_0 \sim N(\mu_0, \sigma^2)$, we further take the natural logarithm of both sides to specialize further x^* with the terms of $(\mu_1, \mu_0, \sigma, \pi_1, \pi_0)$:

$$\ln\left(\frac{\pi_1}{\pi_0}\right) - \frac{(x^*-\mu_1)^2}{2\sigma^2} + \frac{(x^*-\mu_0)^2}{2\sigma^2} = \ln(1-2\rho(\hat{x}^*)).$$

After rearranging, we have the optimal Bayesian decision boundary that maximizes the accuracy on noisy dataset (X, Y^*) as

$$x^* = \frac{1}{2}(\mu_0+\mu_1) + \ln\left(\frac{\pi_0}{\pi_1}\right)\frac{\sigma^2}{\mu_1-\mu_0} + \ln(1-2\rho(x^*))\frac{\sigma^2}{\mu_1-\mu_0}.$$

For the multivariate normal distribution with equal covariance Σ, the decision boundary has the form:

$$2(\mu_1-\mu_0)^T\Sigma^{-1}x^* = \mu_1^T\Sigma^{-1}\mu_1 - \mu_0^T\Sigma^{-1}\mu_0 + 2\ln\left(\frac{\pi_0}{\pi_1}\right) + 2\ln(1-2\rho(x^*)).$$

B. Impact of imbalance ratio on decision boundary of KNN classifier

In this section, we investigate the impact of the imbalance ratio on the k-nearest neighbors (KNN) algorithm, which is a widely used classification method due to its non-parametric nature.

The KNN classifies a new sample based on the majority voting of its k nearest neighbors in the training dataset. Denote $\mathcal{X}_{train}$ and $\mathcal{X}_{test}$ as the training and testing datasets, respectively. For each instance $x_{test} \in \mathcal{X}_{test}$, let $\mathcal{X}_{nn}(x_{test}; k) = \{x^{(1)}, \ldots, x^{(k)}\} \subset \mathcal{X}_{train}$ with corresponding labels $\{Y^{(1)}, \ldots, Y^{(k)}\}$ be its k-nearest neighbors with ascending Euclidean distances. Then, the KNN classifies x_{test} to the positive class if $\frac{1}{k}\sum_{i=1}^{k}\mathbb{I}(Y^{(i)}=1) \geq 0.5$.

We introduce the following setup to study the impact of the imbalance ratio on the KNN classifier. Denote the open Euclidean ball centered at $x \in \mathcal{X}_{test}$ with the radius $r_k(x) = \|x - x^{(k)}\|$ as $B_k(x) = \{x \in \mathcal{X} : ||x - x^{(k)}|| \leq r_k(x)\}$, where $x^{(k)} \in \mathcal{X}_{train}$ is the k-th nearest neighbor of x and $\|\cdot\|$ is the Euclidean distance. Then, the decision boundary of the KNN is defined as $\{x_{knn} \in \mathcal{X} :\ \Pr(x \in B_k(x_{knn}), Y=1) = \Pr(x \in B_k(x_{knn}), Y=0)\}$.

Lemma B.1. *The decision boundary of the KNN is*

$$S^{knn} = \left\{ x_{knn} \in \mathcal{X} : \frac{\int_{B_k(x_{knn})} P_1(x)dx}{\int_{B_k(x_{knn})} P_0(x)dx} = \frac{\pi_0}{\pi_1} \right\}.$$

Proof. The proof of this lemma follows immediately from the facts that $\Pr(x \in B_k(x_{knn}), Y = 1) = \int_{B_k(x_{knn})} P_1(x)dx$ and $\Pr(x \in B_k(x_{knn}), Y = 0) = \pi_0 \int_{B_k(x_{knn})} P_0(x)dx$. □

When the size of the training dataset $n_{train} \to \infty$, $B_k(x_{knn})$ degenerates to the point x_{knn} and $\frac{\int_{B_k(x_{knn})} P_1(x)dx}{\int_{B_k(x_{knn})} P_0(x)dx}$ vanishes to $\frac{P_1(x_{knn})}{P_0(x_{knn})}$. In this case, the decision boundary of the KNN coincides with the Bayesian decision boundary, so the imbalance ratio has the same impact on the decision boundary of the KNN as for the Bayesian decision boundary. In the case of a finite training size, the KNN decision boundary may deviate from the Bayesian decision boundary as demonstrated in the following example.

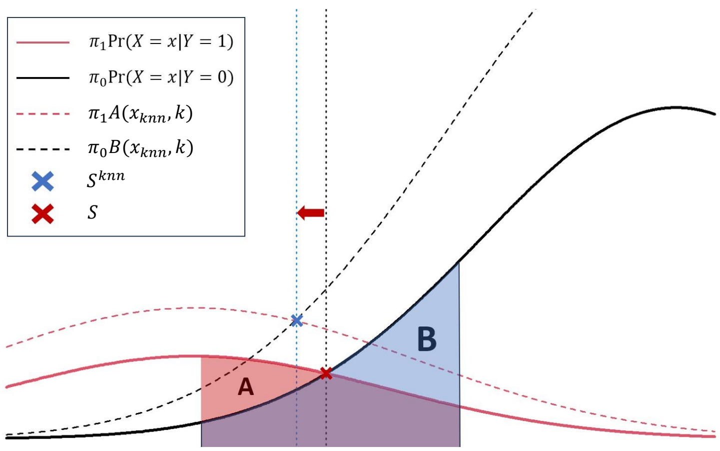

Figure 5: KNN biases the decision boundary from the optimal Bayesian decision boundary towards the minority class region when data is imbalanced. Area A and area B are calculated by assuming $r_k(x^*) = 1$ and substituting $x = x^*$ and $r_k(x^*) = 1$ into $A_1(x, k)$ and $A_0(x, k)$ respectively.

Example 3. *For one-dimensional data, $B_k(x_{knn})$ is an interval on the x-axis of length $2r_k(x_{knn})$. The theoretical decision boundary produced by the KNN classifier has the following form*

$$S^{knn} = \left\{ x_{knn} \in \mathcal{X} : \frac{A_1(x_{knn}, r)}{A_0(x_{knn}, r)} = \frac{\pi_0}{\pi_1} \right\}. \tag{6}$$

where $A_1(x_{knn}, r) = \int_{x-r_k(x_{knn})}^{x+r_k(x_{knn})} P_1(x)dx$, and $A_0(x_{knn}, r) = \int_{x-r_k(x_{knn})}^{x+r_k(x_{knn})} P_0(x)dx$ represent the areas under the class-conditional probability density curves.

Let $P_1 \sim N(0, 1)$, $P_0 \sim N(2.5, 1)$ with $\pi_1 = 0.2$ and $\pi_0 = 0.8$ as considered in Figure 5, the Bayesian decision boundary is $S = x^* \in \mathcal{X} : x^* = 0.6955$ (the red cross). With $r_k(x^*) = 1$, we obtain area A: $\pi_1 A_1(0.6955, k) = 0.1147$ and area B: $\pi_0 A_0(0.6955, k) = 0.1674$, thus $A < B$ indicating that the decision boundary of KNN biases from the Bayesian decision boundary towards the minority class.

As the KNN decision boundary S^{knn} does not have an explicit expression due to $r_k(x^*)$ being dependent on both x^* and k, we numerically demonstrate the relation between $r_k(x^*)$ and the deviation of x^*_{knn} and x^* in Figure 6. From Figure 6, it is evident that the decision boundary x^*_{knn} of KNN deviates from the optimal decision boundary x^* as $r_k(x^*)$ increases on imbalanced data, while it consistently aligns with x^* on balanced data for this example.

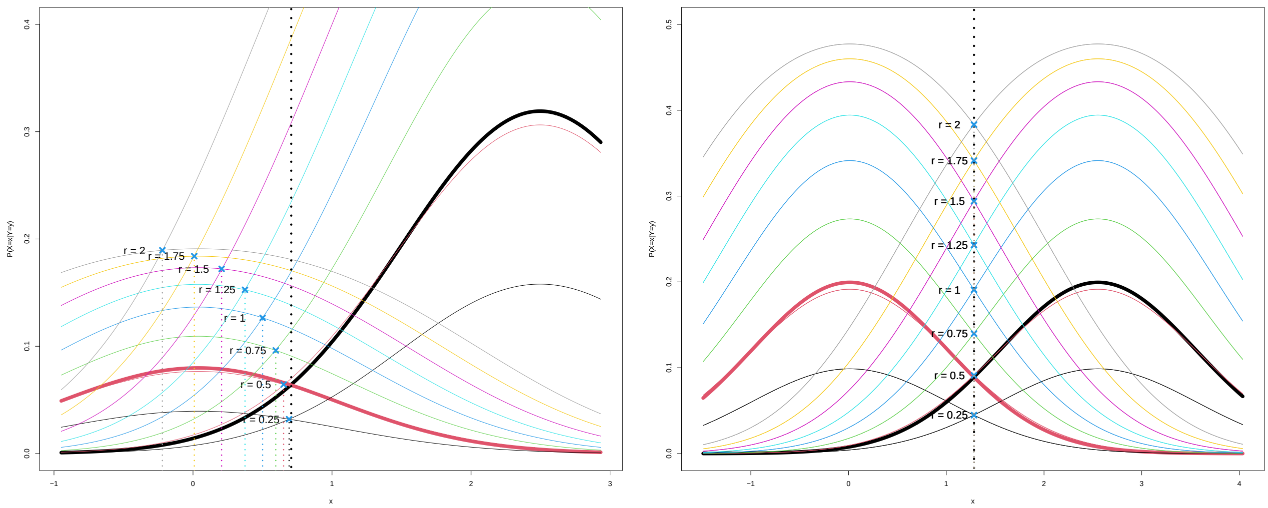

(a) KNN on imbalanced data

(b) KNN on balanced data

Figure 6: The thin curves in different colors represent $\pi_1 A(x, r_k)$ and $\pi_0 B(x, r_k)$ with different values of $r_k = r$. Their intersections (blue cross) are the decision boundaries produced by KNN with the corresponding r value, and the optimal Bayesian decision boundary $x = x^*$ is shown with the vertical dashed black line.

The Bayesian decision boundary tends to be biased towards the minority class region in comparison to the optimal F1 score decision boundary, thereby contributing to a decrease in F1 score performance. Additionally, the decision boundary fitted by the KNN classifier exhibits a continued encroachment upon the minority class region, resulting in compromised accuracy and F1 score performance.

C. Experiment details and full results

C.1. Compute resources

Hardware information. **Type of CPU:** One Intel(R) Core(TM) i7-10700K CPU @ 3.80GHz with 16 cores. **Type of GPU:** One NVIDIA GeForce RTX 4080 SUPER with memory of 16GB.

Computational workload. The experiments on 8 synthetic datasets are repeated 30 rounds using 3 different classifiers with 8 methods. The total amount of training is $8 \times 30 \times 3 \times 8 = 5760$ for experiments on synthetic data. The experiment conducted on CIFAR-10/100 involves 5 methods in 2 different imbalanced settings. The results are collected from 10 rounds of training with 100 epochs. The total epochs of training is $5 \times 2 \times 10 \times 100 = 10000$. The experiments on 32 KEEL datasets are repeated in 100 rounds. The total amount of training is $8 \times 100 \times 3 \times 8 = 19200$.

Implementation code for LNR. Code: `https://github.com/guangzhengh/LNR.git`

C.2. Method parameters

The hyperparameters of classifiers are listed in Table 5. Re-sampling methods are compared and implemented using the "imbalanced-learn" package [1] in Python. Classifers KNN, CART, and MLP are implemented with the Python "scikit-learn" package [2], and parameters not listed are set to their default values. The Resnet-32 is implemented with Pytorch.

The parameters are selected within the tuning range in Table 5 by repeating 3 times of 4-fold cross-validation on reshuffled data with F1 score. The KNN-based resampling methods, including SMOTE, ADASYN, Borderline-SMOTE, and CC

[1] `https://github.com/scikit-learn-contrib/imbalanced-learn.git`
[2] `https://github.com/scikit-learn/scikit-learn`

Table 5: Hyperparameters of methods and classifiers

Classifiers	parameter	value	
KNN	k	[5,10]	
MLP	Hidden layer shape	5x10x5	
	Maximum training epochs	800 on synthetic data, 2000 on KEEL data	
	Optimizer	Adam	
	Learning rate	0.001	
Methods	**parameter**	**tuning range**	**steps**
LNR	threshold t_{flip}	[0,4]	10
	training epoch e	[100,4000]	3
KNN-based resampling	k	[1,$\texttt{min}$(20,$N_{minority}$)]	3
OSS	n_{oss}	[2,30]	10
All resampling methods	re-balance ratio γ	[$\frac{\pi_1}{\pi_0}$, 1]	10

(ClusterCentroids), require the user to preset the value k to synthetic or rank the samples.

We introduce deferred label noise after training epoch T_D for multi-class image classification. We set $T_D = 80$ and $t_{flip} = 3.5$ for both imbalance settings on CIFAR-10/100 datasets. For all experiments, the Resnet-32 is trained up to 100 epochs using SDG (stochastic gradient descend) optimizer with a momentum of 0.9 and a learning rate of 0.1 for the first 60 epochs, 0.01 for the epochs 60-80, and 0.0001 after the 80 epochs.

For experiments based on MiSLAS (Zhong et al., 2021), we compare ReMix, SelMix, and LNR in the fine-tune stage of MiSLAS (stage-2) with its default implementation and hyperparameters. The detailed implementation can be accessed through the GitHub URL in Appendix C.1

C.3. Sensitivity analysis

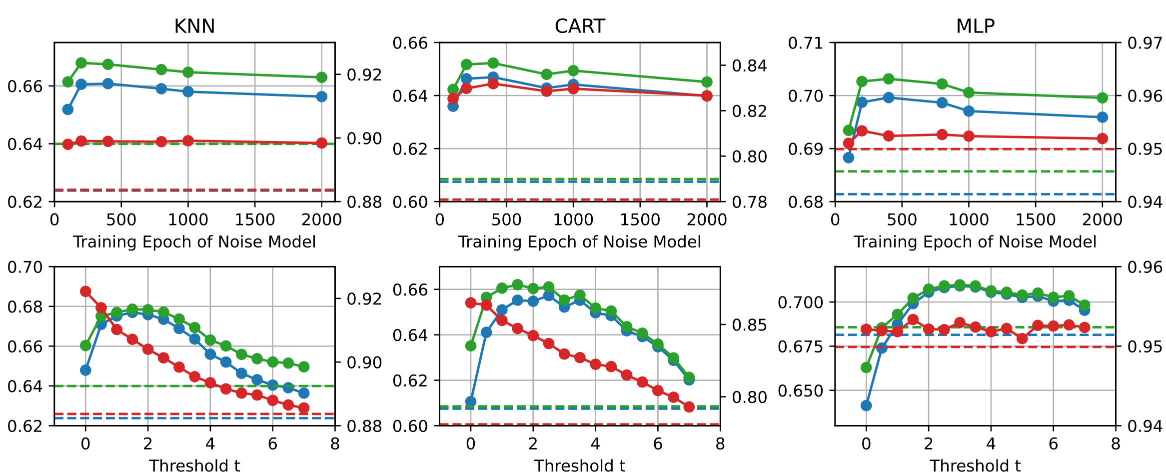

Figure 7: **Sensitivity Analysis.** The horizontal dashed lines represent the baseline performance in terms of F1 (blue), G-mean (green), and AUC (red). The right y-axis corresponds to the AUC values. The solid line denotes the performance of LNR. **Top:** Minimal impact of noise model training epochs on performance gains, with LNR consistently outperforming the baseline. When the number of training epochs is too low (not converged) or too high (overfitting), performance slightly declines. **Bottom:** When the label flip threshold t is too low, we observe poorer performance on MLP compared to the baseline, indicating that a low t leads to excessive noise being introduced. When t is too high, only a few samples are flipped until the performance gain approaches zero. For KNN and CART, the AUC gradually decreases as t increases but not sensitive to MLP.

Sensitivity analysis for each hyperparameter was conducted using simulated data while keeping other parameters constant. In the simulations on synthetic data, the minority class prior was set to 0.1, with a sample size of 500, a class mean distance of 2, and a dimensionality of 5. The results consistently showed that the performance gains from our LNR approach decrease if the threshold is either too low or too high. For KNN and CART, the classifiers always outperformed the baseline regardless of t_{flip}. However, for MLP, if t_{flip} is too low, excessive label noise can cause performance to fall below baseline levels, while if is too high, performance can degrade to baseline levels.

The impact of the epoch parameter on performance is less sensitive. We observed that if the noise model is trained for too few epochs, the benefits of flipped labels are reduced. However, once the model converges, further training does not significantly enhance performance, as the model possesses enough capability to filter out detrimental label noise. As LNR is data-driven, the parameters can be optimized using standard cross-validation techniques like other data-level methods.

The impact of data characteristics on performance. We conduct the experimental analysis on synthetic datasets with different data characteristics with respect to **sample size** and **minority class prior** to provide a better understanding of how data characteristics affect the performance of LNR, shown in 8. As a simple conclusion, our method consistently outperforms other methods under various data characteristics, especially for larger sample sizes and higher imbalance ratios.

C.4. Class Fairness of LNR on long-tailed data

For multi-classification problems, LNR significantly improves the performance in terms of overall accuracy and few-shot accuracy while maintaining class fairness. LNR flip samples are based on the similarity to the minority class, making these flips regulated and self-limiting. This prevents the model from having an unintended bias towards specific classes. To clearly demonstrate the harmfulness of LNR towards class fairness, we compared the average confusion matrices of GCL and GCL-LNR.

Table 6: Conn fusion matrix of GCL-LNR. The differences (higher than 10) compared to the confusion matrix of GCL are reported in the brackets. The horizontal axis represents the predicted value, whereas the vertical axis represents the true value.

GCL-LNR (Differ)	0	1	2	3	4	5	6	7	8	9
0	**908 (-26)**	10	24	8	4	2	2	4	20 (+13)	19 (+16)
1	6	**978 (-4)**	0	0	1	0	1	0	0	13
2	33	3	**860 (-4)**	28	20	21	23	8	0	4
3	23	4	50	**782 (+18)**	25	72 (-13)	22	13	2	8
4	12	2	54	39	**829 (+3)**	16	18	25	2	2
5	15	2	42	140	26	**736 (-1)**	13	24	1	2
6	11	6	58	68	13	14	**820 (-4)**	8	1	1
7	22	3	33	50 (-20)	48	50	6	**778 (+22)**	2	8
8	112 (-91)	52	22	11	2	4	4	2	**758 (+80)**	33 (+20)
9	30 (-42)	148 (-48)	4	8	2	0	3	4	10	**792 (+102)**

The bold numbers on the diagonal demonstrate that LNR achieves a more effective trade-off between the classification performance of the head class and the tail class, using only a small number of head class samples (reduced 16 true positives in head classes [0,1,2,3]) to achieve a significant improvement in tail class performance (increasing 204 true positives in tail classes [7,8,9]). To provide a straightforward understanding of how LNR achieves the better decision boundary on the long-tailed CIFAR-10, we present the statistics of flipped labels below, where "$\rightarrow$" means "flipped to":

$\{$0: [$\rightarrow$7: 2, $\rightarrow$8: 41, $\rightarrow$9: 44], 1:[$\rightarrow$9: 6], 2: [], 3: [], 4: [], 5: [], 6: [], 7: [], 8: [], 9: []$\}$

The long-tailed CIFAR-10 before and after flipping labels by LNR:

Before: 0: 5000, 1: 2997, 2: 1796, 3: 1077, 4: 645, 5: 387, 6: 232, 7: 139, 8: 83, 9: 50

After: 0: 4913, 1: 2991, 2: 1796, 3: 1077, 4: 645, 5: 387, 6: 232, 7: 141, 8: 124, 9: 100

These beneficial label noises effectively correct the classifier's decision boundaries with minimal data editing.

C.5. Experiment datasets

Synthetic data: The simulations are conducted on the d-dimensional Gaussian distribution $N(\mu_r, \Sigma)$, with the mean of μ_r and the covariance matrix Σ being the $d \times d$ identity matrix $\mathcal{I}_d$. We generate the simulated data with the setting: let $\Pr(Y = 1) = \pi_1 \in [0, 1]$ and $X \mid Y = r \sim N(\mu_r, \Sigma)$, where $\mu_1 = (\mu/2, 0, \ldots, 0)^T = -\mu_0 \in \mathbb{R}^d$. There are $2 \times 2 \times 2 = 8$ different distributions generated with different statistical parameters combinations of $|\mu_1 - \mu_0| \in \{1, 2\}$, $d \in \{5, 25\}$, and $\pi_1 \in \{0.1, 0.3\}$. The maximum training epoch of the MLP classifier is set to 800 as MLP converges faster on synthetic datasets. Due to the limited performance on high dimensional synthetic data with the constrained structure of the MLP classifier, we instead use the KNN classifier with $k = 50$ as the flip-rate estimator C_f for LNR on $d = 25$ synthetic datasets.

KEEL dataset: The KEEL repository (Derrac et al., 2015) provides us with 99 binary imbalanced datasets. We select 32 datasets with the following criteria to avoid meaningless and inefficient comparisons on the datasets:

a) Baseline already achieves an F1-score over 90%, or all methods have an F1-score lower than 10%.

b) Datasets with insufficient minority class sample size in the test dataset (less than 10).

The imbalance ratios π_0/π_1 in the selected 32 datasets widely ranged from 1.82 to 49.6, providing a comprehensive comparison. We simply removed all categorical attributes to simplify data preprocessing and standardized the remaining numerical dimensions.

C.6. KEEL Dataset Characteristics

As we discussed in Section 3.2, the degree of decision boundary deviation is affected by both the imbalanced ratio and the class overlap. The indicator of the imbalance ratio is less insightful as the degree of class overlap may vary largely on datasets of the same imbalance ratio. To study the methods' strengths and weaknesses, we summarise the characteristics of the dataset based on the categories proposed by (Napierala & Stefanowski, 2016), which suggests assigning each minority class sample to one of the following groups based on the number of minority class neighbors within the 5-nearest-neighbors: **Safe:** $4+$, **Border:** $2-3$, **Rare:** 1, **Outlier:** 0. The proportion of each group describes the distribution of minorities in the imbalanced dataset, especially Border and Rare reflecting the extent of class overlap, as a complementary metric to the imbalanced ratio.

C.7. Evaluation settings and results

Settings. We employed various seeds to generate 30 sets of synthetic training and testing datasets, with the sample size $N_{train} = 500$ and $N_{test} = 2000$ for all 8 distributions. Due to the limited sample size for the KEEL datasets, we use different seeds to partition the data into 100 sets of training and testing datasets at a ratio of 7:3, ensuring at least 10 minority class samples in each testing set. With 30 rounds on synthetic data and 100 rounds on KEEL datasets, we obtain statistically significant results, and the mean and the standard deviation are reported in Appendix C.7.

Metrics. The performance on binary classification is evaluated in three different metrics: F1 score, G-mean (Geometric Mean), and AUC (Area under the Curve). Different to the definition of F1, which mainly focuses on the true positives, G-mean also considers the true negatives with the following definition:

$$\text{G-mean} = \sqrt{\frac{\text{TP}}{\text{TP}+\text{FN}} \times \frac{\text{TN}}{\text{TN}+\text{FP}}}.$$

Compared to accuracy, AUC evaluates the classification performance of a classifier by calculating the area under the ROC (Receiver Operating Characteristic) curve. The ROC curve takes into account both recall (TPR) and FPR (False Positive Rate), defined as:

$$\text{AUC} = \int_0^1 \text{TPR}(\text{FPR}^{-1}(t))dt$$

where $\text{FPR} = \text{FP}/(\text{FP} + \text{TN})$. A classifier that correctly classifies positive samples as positive while maintaining a low error rate for negative samples will have a higher AUC. Unlike F1 and G-mean, which are more sensitive to the prediction performance of minority class samples, AUC is a more conservative metric for comprehensively reflecting the performance of a classifier. Methods that significantly increase the number of minority class samples to improve F1 score or G-mean often come at the cost of higher errors in negative samples (FP). Therefore, we desire a re-balancing method that should consider these three metrics comprehensively.

For multi-class image classification, we use different metrics to evaluate the performance on step-wise and long-tailed datasets. On the step-wise CIFAR-10/100, due to half of classes are removed 99% of samples forms 5 and 50 minority classes, we evaluated model by the average accuracy of minority classes denoted as $\text{Recall}_{\text{MI}}$ and the average precision of majority classes denoted as Preci_{MA}, as well as the overall accuracy. For long-tailed CIFAR-10, we report the average accuracy across *Many-shot* ($N_c > 1000$), *Many-shot* ($100 \geq N_c \geq 200$), and *Few-shot* ($N_c < 2000$), where $N_C = [5000, 2997, 1796, 1077, 645, 387, 232, 139, 83, 50]$. For long-tailed CIFAR-100, we define the *Many-shot* ($N_c > 200$), *Many-shot* ($200 \geq N_c \geq 20$), and *Few-shot* ($N_c < 20$).

Results on synthetic datasets. The 8 synthetic datasets vary in degrees of class overlap, imbalance ratio, and dimensionality. Table 8 presents the case of $\pi_1 = 0.1$, $d = 25$, $\mu_D = 2$. Our approach consistently outperformed other methods across all datasets for both F1 score and G-mean, achieving the best AUC performance for most datasets. Through the relative performance ranking shown in Figure 9, our approach achieves the highest ranks across all metric classifiers, demonstrating its overall superiority over resampling methods on all metrics. The synthetic Gaussian distributional dataset results with 3 classifiers are reported in Table 12, where each row represents the (average ± std) result of 30 rounds on the distribution with different statistical settings. The win-times on synthetic datasets are reported in Table 9. The numerical results are reported in Table 10.

Results on KEEL datasets. The comparison results on the KEEL datasets are reported in Tables 13–21 in the format of (average% ± std) of 100 rounds for each dataset, demonstrating the superiority of our method on KEEL datasets. The win-times of each methods for each classifier on each metric are summarized below and the highest value of each column are in bold:

In order to provide a deeper understanding of the strengths and weaknesses of our method, we calculate the relative performance difference as an extension to the relative rankings. The relative performance differences between our method and re-sampling methods are calculated by: 1) First we min-max normalize the result of all methods on each dataset and obtain the relative performances. 2) Minus the relative performance of our method to calculate the differences. We then calculate the Pearson correlation coefficients between the relative performance differences and the minority class sample distribution characteristics {safe, border, rare, outlier} is shown in Table 11. Coefficients higher than 0.25 or lower than -0.25 are highlighted with bold fonts.

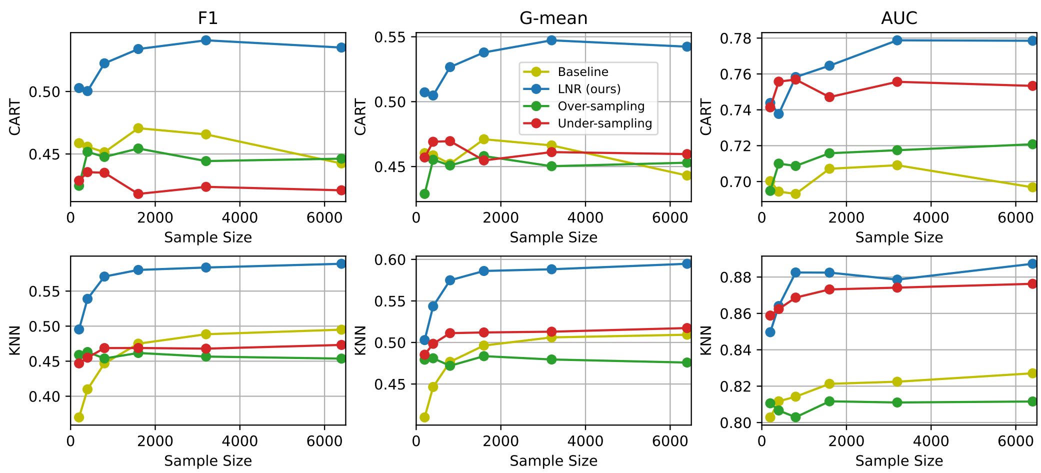

(a) Sample Size

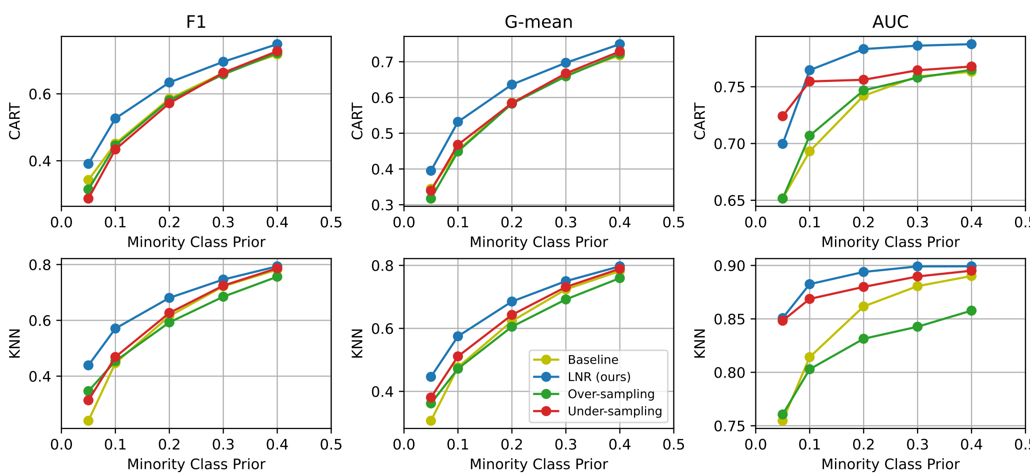

(b) Minority Class Prior

Figure 8: **The impact of data characteristics on performance**. For clarity, the average performance of over-sampling and under-sampling methods is reported. **a)** Our method demonstrates performance gains comparable to those of resampling methods when the sample size is 200. However, our method consistently outperforms the others as the sample size increases. **b)** As the data approaches a more balanced state, all methods exhibit similar performance; notably, our method's AUC shows improvement even with more balanced data. The performance gains of our method in terms of F1 and G-mean become more evident as the prior of the minority class decreases.

Table 7: KEEL(Derrac et al., 2015) Data statistics and characteristics: d is the number of dimensions, N_1 and N_0 denote the number of minority and majority class samples.

statistics					
index	Dataset Name	d	(N, N_1, N_0)	IR: π_0/π_1	(S,B,R,O)
1	*abalone-17_vs_7-8-9-10*	7	(2338, 58, 2280)	39.31	(0.02, 0.22, 0.33, 0.43)
2	*abalone-19_vs_10-11-12-13*	7	(1622, 32, 1590)	49.69	(0.0, 0.0, 0.28, 0.72)
3	*abalone9-18*	7	(731, 42, 689)	16.4	(0.02, 0.4, 0.17, 0.4)
4	*ecoli1*	7	(336, 77, 259)	3.36	(0.53, 0.32, 0.08, 0.06)
5	*ecoli2*	7	(336, 52, 284)	5.46	(0.77, 0.15, 0.0, 0.08)
6	*ecoli3*	7	(336, 35, 301)	8.6	(0.29, 0.49, 0.09, 0.14)
7	*flare-F*	9	(1066, 43, 1023)	23.79	(0.05, 0.26, 0.4, 0.3)
8	*glass-0-1-2-3_vs_4-5-6*	9	(214, 51, 163)	3.2	(0.67, 0.22, 0.06, 8.06)
9	*glass0*	9	(214, 70, 144)	2.06	(0.56, 0.36, 0.03, 0.06)
10	*glass1*	9	(214, 76, 138)	1.82	(0.46, 0.3, 0.16, 0.08)
11	*haberman*	3	(306, 81, 225)	2.78	(0.05, 0.47, 0.32, 0.16)
12	*kr-vs-k-three_vs_eleven*	3	(2935, 81, 2854)	35.23	(0.62, 0.22, 0.09, 0.07)
13	*kr-vs-k-zero-one_vs_draw*	3	(2901, 105, 2796)	26.63	(0.65, 0.23, 0.06, 0.07)
14	*led7digit-0-2-4-5-6-7-8-9_vs_1*	7	(443, 37, 406)	10.97	(0.19, 0.65, 0.14, 0.03)
15	*newthyroid2*	5	(215, 35, 180)	5.14	(0.69, 0.31, 0.0, 0.0)
16	*page-blocks0*	10	(5472, 559, 4913)	8.79	(0.7, 0.17, 0.07, 0.06)
17	*pima*	8	(768, 268, 500)	1.87	(0.3, 0.45, 0.17, 0.09)
18	*vehicle1*	18	(846, 217, 629)	2.9	(0.24, 0.57, 0.15, 0.05)
19	*vehicle3*	18	(846, 212, 634)	2.99	(0.16, 0.51, 0.26, 0.06)
20	*yeast-0-2-5-6_vs_3-7-8-9*	8	(1004, 99, 905)	9.14	(0.35, 0.3, 0.15, 0.19)
21	*yeast-0-2-5-7-9_vs_3-6-8*	8	(1004, 99, 905)	9.14	(0.68, 0.17, 0.05, 0.1)
22	*yeast-0-3-5-9_vs_7-8*	8	(506, 50, 456)	9.12	(0.16, 0.28, 0.22, 0.34)
23	*yeast-0-5-6-7-9_vs_4*	8	(528, 51, 477)	9.35	(0.08, 0.43, 0.18, 0.31)
24	*yeast-1-2-8-9_vs_7*	8	(947, 30, 917)	30.57	(0.0, 0.27, 0.23, 0.5)
25	*yeast-1-4-5-8_vs_7*	8	(693, 30, 663)	22.1	(0.0, 0.07, 0.43, 0.5)
26	*yeast-1_vs_7*	7	(459, 30, 429)	14.3	(0.07, 0.33, 0.27, 0.33)
27	*yeast-2_vs_4*	8	(514, 51, 463)	9.08	(0.55, 0.22, 0.06, 0.18)
28	*yeast1*	8	(1484, 429, 1055)	2.46	(0.21, 0.45, 0.22, 0.11)
29	*yeast3*	8	(1484, 163, 1321)	8.1	(0.56, 0.26, 0.08, 0.1)
30	*yeast4*	8	(1484, 51, 1433)	28.1	(0.06, 0.35, 0.2, 0.39)
31	*yeast5*	8	(1484, 44, 1440)	32.73	(0.34, 0.5, 0.11, 0.05)
32	*yeast6*	8	(1484, 35, 1449)	41.4	(0.37, 0.23, 0.11, 0.29)

Table 8: Results on synthetic data with $\pi_1 = 0.1$, $d = 25$, $\mu_D = 2$ (average % ±std).

Metric	Classifier	baseline	**LNR**	Over-sampling			Under-sampling		
				SMOTE	ADASYN	Borderline	OSS	CC	RUS
F1 score	KNN	15.72±0.05	**40.88±0.04**	31.63±0.03	31.15±0.03	33.4 ±0.03	24.94±0.07	27.1 ±0.07	35.74±0.04
	CART	43.72±0.05	**49.52±0.03**	40.56±0.05	39.48±0.05	40.51±0.05	42.59±0.06	36.3 ±0.04	38.94±0.05
	MLP	44.32±0.05	**47.82±0.03**	42.68±0.05	42.35±0.04	44.01±0.04	43.39±0.04	28.84±0.02	30.44±0.04
G-mean	KNN	23.89±0.05	**43.28±0.03**	37.86±0.02	37.5±0.02	38.28 ±0.03	29.07±0.06	33.54±0.06	41.48±0.03
	CART	43.88±0.05	**50.5 ±0.03**	41.08±0.05	39.86±0.05	40.79±0.05	43.07±0.05	43.73±0.03	44.29±0.05
	MLP	44.55±0.04	**48.87±0.03**	42.95±0.05	42.62±0.04	44.18±0.04	43.62±0.04	35.61±0.02	36.26±0.04
AUC	KNN	71.06±0.03	**81.53±0.03**	73.98±0.02	73.52±0.03	74.5 ±0.02	73.33±0.03	74.41±0.03	80.29±0.03
	CART	69.04±0.03	75.58±0.03	68.67±0.03	67.88±0.03	67.96±0.04	69.72±0.03	**75.77±0.03**	75.45±0.04
	MLP	82.52±0.03	**84.6 ±0.02**	79.94±0.04	79.77±0.04	80.25±0.04	81.13±0.03	73.5 ±0.03	74.01±0.05

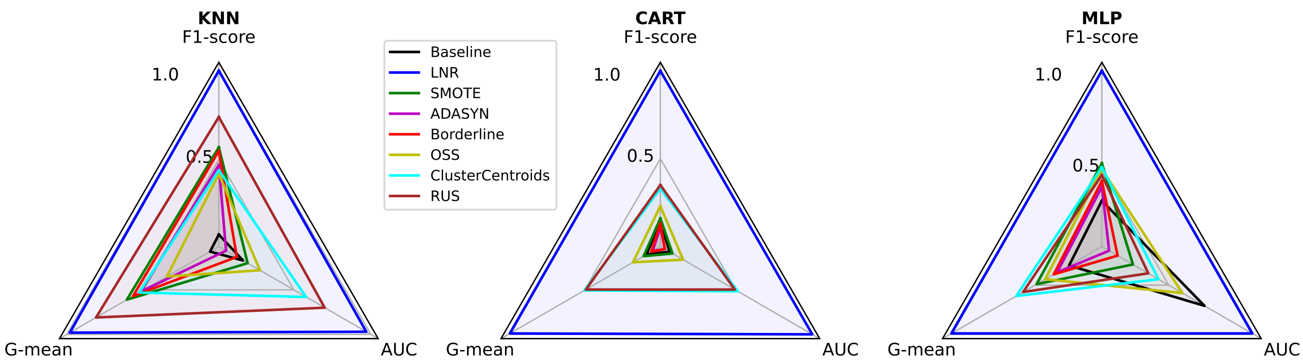

Figure 9: Relative ranking of methods from 1 (the best) to 0 (the lowest) on 8 synthetic datasets.

Table 9: Win-times comparison on **8 Synthetic datasets / 32 KEEL datasets**.

	KNN			CART			MLP		
methods	F1	G-mean	AUC	F1	G-mean	AUC	F1	G-mean	AUC
baseline	0/ 2	0/ 2	0/ 1	0/ 4	0/ 4	0/ 1	0/ 2	0/ 2	2/**13**
LNR	**8/16**	**6/16**	**7**/ 9	**8/21**	**8/18**	**8/13**	**8/19**	**8/16**	**6**/ 5
SMOTE	0/ 5	0/ 5	0/ 2	0/ 3	0/ 3	0/ 1	0/ 2	0/ 1	0/ 7
ADASYN	0/ 3	0/ 2	0/ 0	0/ 2	0/ 2	0/ 2	0/ 3	0/ 3	0/ 2
Borderline	0/ 4	0/ 4	0/ 0	0/ 1	0/ 1	0/ 0	0/ 4	0/ 4	0/ 2
OSS	0/ 2	0/ 2	0/ 0	0/ 1	0/ 1	0/ 2	0/ 2	0/ 2	0/ 1
CC	0/ 0	0/ 1	0/**19**	0/ 0	0/ 2	0/ 2	0/ 0	0/ 3	0/ 2
RUS	0/ 0	2/ 0	1/ 1	0/ 0	0/ 1	0/11	0/ 0	0/ 1	0/ 0

Table 10: Relative performance ranking on 8 synthetic and 32 KEEL datasets

				Over-sampling		Under-sampling			
Classifiers	Metrics	baseline	**LNR**	SMOTE	ADASYN	Borderline	OSS	CC	RUS
				Synthetic Gaussian datasets					
KNN	F1	0.08	**1.**	0.57	0.47	0.55	0.42	0.44	0.74
	G-mean	0.07	**0.98**	0.61	0.52	0.57	0.35	0.53	0.81
	AUC	0.17	**0.97**	0.2	0.06	0.13	0.28	0.58	0.7
CART	F1	0.15	**1.**	0.16	0.11	0.13	0.23	0.33	0.35
	G-mean	0.09	**0.99**	0.11	0.05	0.06	0.18	0.5	0.49
	AUC	0.06	**1.**	0.08	0.03	0.03	0.15	0.51	0.49
MLP	F1	0.34	**1.**	0.53	0.41	0.44	0.5	0.51	0.47
	G-mean	0.3	**0.99**	0.49	0.37	0.39	0.44	0.61	0.57
	AUC	0.71	**0.99**	0.29	0.15	0.2	0.58	0.44	0.38
				KEEL datasets					
KNN	F1	0.35	**0.86**	0.69	0.59	0.75	0.53	0.32	0.37
	G-mean	0.33	**0.84**	0.65	0.53	0.7	0.5	0.4	0.43
	AUC	0.42	0.7	0.34	0.2	0.22	0.3	**0.79**	0.66
CART	F1	0.58	**0.93**	0.56	0.51	0.54	0.56	0.19	0.39
	G-mean	0.5	**0.89**	0.46	0.37	0.43	0.47	0.29	0.5
	AUC	0.31	**0.82**	0.4	0.32	0.35	0.48	0.43	0.72
MLP	F1	0.36	**0.91**	0.72	0.65	0.75	0.48	0.34	0.35
	G-mean	0.35	**0.9**	0.69	0.61	0.73	0.44	0.41	0.44
	AUC	**0.81**	0.8	0.64	0.46	0.46	0.45	0.41	0.39

Table 11: Pearson Correlation between data distribution characteristics and relative performance differences

			Over-sampling			Under-sampling		
Metrics	Characteristics	baseline	SMOTE	ADASYN	Borderline	OSS	CC	RUS
		with **KNN** classifier						
F1-score	Dimension	**0.3**	0.16	0.01	0.08	0.1	-0.13	-0.12
	IR	-0.03	-0.08	-0.14	-0.13	0.16	0.17	0.34
	Safe	**-0.77**	-0.18	0.06	-0.03	**-0.71**	-0.06	0.04
	Border	**0.26**	0.16	0.04	0.17	**0.26**	0.18	-0.03
	Rare	**0.68**	0.08	-0.13	0.02	**0.68**	0.01	-0.12
	Outlier	**0.48**	0.07	-0.04	-0.11	**0.39**	-0.05	0.04
G-mean	Dimension	**0.32**	0.14	-0.01	0.06	0.12	-0.1	-0.1
	IR	-0.02	-0.07	-0.1	-0.08	0.09	0.04	0.13
	Safe	**-0.76**	-0.23	-0.02	-0.12	**-0.63**	0.09	0.22
	Border	**0.3**	0.16	0.04	0.12	**0.31**	0.25	0.08
	Rare	**0.69**	0.15	-0.06	0.13	**0.63**	-0.16	-0.32
	Outlier	**0.43**	0.1	0.02	-0.01	**0.27**	-0.23	-0.19
AUC	Dimension	0.1	**0.31**	0.24	**0.31**	0.21	**0.27**	0.47
	IR	**0.49**	0.21	0.05	0.1	**0.3**	-0.23	-0.18
	Safe	**-0.56**	**-0.53**	**-0.33**	**-0.43**	**-0.57**	**-0.28**	-0.3
	Border	-0.06	0.23	0.17	0.22	0.1	**0.31**	0.22
	Rare	**0.44**	**0.39**	0.2	**0.26**	**0.6**	**0.3**	0.29
	Outlier	**0.59**	**0.33**	0.2	**0.27**	**0.38**	-0.03	0.08
		with **CART** classifier						
F1-score	Dimension	**0.4**	**0.29**	**0.26**	**0.27**	**0.31**	0.01	-0.15
	IR	**-0.3**	-0.15	-0.16	-0.15	-0.13	0.18	0.48
	Safe	-0.25	**-0.59**	**-0.57**	**-0.42**	-0.14	-0.12	-0.26
	Border	0.23	**0.27**	0.18	0.21	0.05	-0.04	-0.05
	Rare	**0.32**	**0.63**	**0.59**	**0.42**	0.16	0.07	0.15
	Outlier	-0.03	0.24	**0.3**	0.17	0.06	0.17	0.32
G-mean	Dimension	**0.41**	**0.27**	0.24	**0.26**	**0.33**	0.03	-0.07
	IR	**-0.32**	-0.06	-0.08	-0.12	-0.1	-0.14	-0.05
	Safe	**-0.27**	**-0.66**	**-0.6**	**-0.49**	-0.21	**0.28**	0.24
	Border	**0.32**	**0.31**	0.22	0.23	0.14	0.24	0.31
	Rare	**0.29**	**0.63**	**0.53**	**0.46**	0.21	**-0.36**	-0.33
	Outlier	-0.05	**0.31**	**0.37**	0.24	0.06	**-0.38**	-0.4
AUC	Dimension	**0.39**	**0.41**	**0.34**	**0.36**	**0.32**	0.14	0.05
	IR	-0.24	-0.04	-0.05	-0.07	0.02	**-0.4**	-0.56
	Safe	-0.03	**-0.58**	**-0.41**	**-0.36**	-0.2	0.17	0.29
	Border	0.16	0.23	0.1	0.14	0.12	0.22	0.26
	Rare	0.04	**0.52**	**0.36**	**0.32**	**0.27**	-0.1	-0.19
	Outlier	-0.13	**0.31**	**0.29**	0.2	0.01	**-0.37**	-0.52
		with **MLP** classifier						
F1-score	Dimension	**0.28**	0.04	0.11	0.12	**0.31**	0.01	0.02
	IR	-0.05	0.08	-0.02	0.03	0.03	0.14	0.3
	Safe	**-0.75**	-0.05	0.11	0.02	**-0.46**	0.05	0.04
	Border	**0.38**	-0.24	**-0.29**	-0.2	-0.16	-0.09	-0.09
	Rare	**0.63**	0.13	-0.03	0.06	**0.48**	-0.03	-0.16
	Outlier	**0.39**	0.2	0.09	0.1	**0.5**	0.02	0.11
G-mean	Dimension	**0.31**	0.15	0.14	0.15	**0.29**	0.03	-0.01
	IR	-0.04	-0.02	-0.04	0.03	0.02	0.01	0.15
	Safe	**-0.74**	-0.11	0.06	-0.03	**-0.48**	0.18	0.18
	Border	**0.42**	-0.18	**-0.26**	-0.21	-0.1	-0.02	-0.01
	Rare	**0.59**	0.14	-0.02	0.09	**0.45**	-0.16	-0.32
	Outlier	**0.37**	0.21	0.13	0.16	**0.49**	-0.14	-0.06
AUC	Dimension	-0.25	-0.18	-0.15	0.01	-0.11	0.03	0.1
	IR	-0.07	**0.42**	**0.35**	**0.28**	-0.08	0.12	0.39
	Safe	0.05	**-0.5**	-0.17	**-0.27**	0.13	**-0.43**	-0.56
	Border	-0.21	**-0.28**	**-0.38**	**-0.36**	0.2	0.22	0.19
	Rare	0.05	**0.47**	0.25	**0.35**	-0.2	**0.36**	0.35
	Outlier	0.08	**0.67**	**0.39**	**0.47**	-0.22	0.21	0.44

Table 12: Comparison on synthetic datasets with KNN, CART and MLP classifiers.

	Settings			**Over-sampling**			**Under-sampling**		
Metric	π_1,μ_D,d	baseline	**LNR**	SMOTE	ADASYN	Borderline	OSS	CC	RUS
				with **KNN** classifier					
F1-score	0.1,1,5	8.54±0.03	**29.82±0.03**	22.05±0.02	21.5±0.02	23.24±0.03	12.85±0.04	12.85±0.04	24.94±0.02
	0.1,1,25	2.0±0.01	**21.8±0.03**	19.47±0.01	19.5±0.01	19.86±0.02	5.19±0.03	5.19±0.03	20.73±0.02
	0.1,2,5	43.38±0.06	**55.2±0.04**	44.21±0.03	42.68±0.04	48.07±0.04	47.76±0.05	47.76±0.05	44.86±0.04
	0.1,2,25	15.72±0.05	**40.88±0.04**	31.63±0.03	31.15±0.03	33.4±0.03	24.94±0.07	24.94±0.07	35.74±0.04
	0.3,1,5	39.7±0.03	**54.19±0.02**	47.45±0.02	47.23±0.01	46.67±0.02	45.99±0.02	45.99±0.02	50.38±0.02
	0.3,1,25	27.61±0.03	**48.88±0.02**	45.42±0.02	45.1±0.01	45.08±0.01	36.49±0.03	36.49±0.03	44.05±0.03
	0.3,2,5	71.14±0.03	**73.64±0.02**	70.6±0.02	67.82±0.02	68.3±0.02	72.66±0.02	72.66±0.02	72.58±0.02
	0.3,2,25	54.75±0.04	**66.1±0.02**	60.11±0.02	58.13±0.02	58.3±0.02	60.91±0.04	60.91±0.04	64.6±0.02
G-mean	0.1,1,5	12.12±0.04	31.26±0.03	24.57±0.02	24.07±0.02	24.45±0.03	14.83±0.04	**32.86±0.02**	31.4±0.03
	0.1,1,25	3.98±0.02	23.87±0.03	25.43±0.02	25.69±0.02	24.29±0.02	6.97±0.03	8.22±0.04	**26.42±0.03**
	0.1,2,5	46.52±0.05	**56.04±0.04**	46.8±0.03	45.28±0.04	49.29±0.04	49.04±0.05	51.12±0.03	50.49±0.03
	0.1,2,25	23.89±0.05	**43.28±0.03**	37.86±0.02	37.5±0.02	38.28±0.03	29.07±0.06	33.54±0.06	41.48±0.03
	0.3,1,5	40.5±0.02	**55.38±0.02**	48.2±0.02	48.42±0.01	47.51±0.02	46.09±0.02	54.36±0.02	51.63±0.02
	0.3,1,25	29.17±0.03	**51.57±0.03**	49.19±0.03	49.02±0.02	48.73±0.02	36.73±0.03	31.98±0.03	45.34±0.03
	0.3,2,5	71.32±0.03	**74.15±0.02**	71.07±0.02	68.76±0.02	69.08±0.02	72.83±0.02	72.62±0.01	73.3±0.02
	0.3,2,25	56.22±0.03	**67.83±0.02**	63.71±0.02	62.23±0.02	62.42±0.02	61.16±0.04	59.37±0.03	65.98±0.03
AUC	0.1,1,5	60.2±0.02	**69.2±0.02**	60.18±0.02	59.94±0.02	60.98±0.02	60.76±0.03	68.02±0.03	66.35±0.03
	0.1,1,25	54.93±0.02	**61.36±0.03**	55.74±0.02	55.65±0.02	56.33±0.03	55.75±0.02	57.04±0.03	59.14±0.03
	0.1,2,5	81.19±0.02	87.1±0.03	80.69±0.02	79.74±0.02	80.93±0.02	82.34±0.02	**89.67±0.01**	88.16±0.02
	0.1,2,25	71.06±0.03	**81.53±0.03**	73.98±0.02	73.52±0.03	74.5±0.02	73.33±0.03	74.41±0.03	80.29±0.03
	0.3,1,5	65.27±0.01	**71.54±0.02**	63.95±0.02	62.81±0.02	63.11±0.02	65.92±0.01	67.96±0.02	67.15±0.02
	0.3,1,25	57.36±0.01	**64.54±0.02**	56.55±0.03	55.12±0.02	55.87±0.02	57.7±0.01	58.9±0.01	59.22±0.02
	0.3,2,5	87.83±0.02	**89.63±0.01**	86.49±0.02	84.21±0.01	84.06±0.02	88.35±0.02	89.38±0.01	89.34±0.01
	0.3,2,25	78.82±0.02	**85.49±0.01**	81.36±0.02	79.58±0.03	79.64±0.03	79.79±0.03	80.22±0.02	83.31±0.02
				with **CART** classifier					
F1-score	0.1,1,5	19.13±0.04	**27.94±0.03**	19.22±0.02	19.5±0.03	18.83±0.03	19.22±0.03	23.07±0.03	22.21±0.02
	0.1,1,25	16.3±0.03	**24.07±0.03**	17.6±0.03	17.02±0.03	16.7±0.03	17.3±0.02	21.66±0.02	21.29±0.02
	0.1,2,5	44.77±0.05	**52.49±0.04**	44.49±0.05	42.96±0.06	44.43±0.05	43.96±0.05	41.99±0.06	39.6±0.05
	0.1,2,25	43.72±0.05	**49.52±0.03**	40.56±0.05	39.48±0.05	40.51±0.05	42.59±0.06	36.3±0.04	38.94±0.05
	0.3,1,5	41.07±0.02	**52.0±0.02**	42.24±0.02	42.64±0.02	42.16±0.02	43.98±0.02	45.33±0.02	46.14±0.02
	0.3,1,25	40.11±0.02	**50.01±0.02**	40.53±0.03	40.84±0.02	40.48±0.03	41.32±0.02	45.38±0.02	44.6±0.02
	0.3,2,5	65.66±0.02	**71.68±0.02**	66.03±0.02	65.0±0.02	65.93±0.02	66.88±0.02	66.32±0.02	67.12±0.03
	0.3,2,25	64.18±0.02	**69.7±0.02**	64.02±0.02	63.39±0.02	63.38±0.03	64.75±0.02	64.63±0.02	65.37±0.02
G-mean	0.1,1,5	19.22±0.04	**30.48±0.03**	19.76±0.02	19.91±0.03	19.05±0.03	19.58±0.03	28.41±0.03	28.39±0.02
	0.1,1,25	16.42±0.03	27.33±0.04	18.09±0.03	17.48±0.03	16.98±0.03	17.81±0.02	**28.68±0.02**	26.68±0.03
	0.1,2,5	44.91±0.05	**53.83±0.03**	44.97±0.05	43.49±0.06	44.68±0.05	44.51±0.05	46.82±0.05	45.28±0.04
	0.1,2,25	43.88±0.05	**50.5±0.03**	41.08±0.05	39.86±0.05	40.79±0.05	43.07±0.05	43.73±0.03	44.29±0.05
	0.3,1,5	41.11±0.02	**53.42±0.02**	42.38±0.02	42.88±0.02	42.26±0.02	44.29±0.02	46.29±0.02	47.29±0.03
	0.3,1,25	40.15±0.02	**51.55±0.02**	40.73±0.03	41.01±0.02	40.63±0.03	41.57±0.03	46.55±0.02	45.61±0.02
	0.3,2,5	65.69±0.02	**72.29±0.02**	66.13±0.02	65.13±0.02	66.02±0.02	67.09±0.02	66.86±0.02	67.73±0.03
	0.3,2,25	64.21±0.02	**70.24±0.02**	64.15±0.02	63.51±0.02	63.51±0.03	64.92±0.02	65.36±0.02	65.88±0.02
AUC	0.1,1,5	55.11±0.02	**62.86±0.02**	55.06±0.02	55.22±0.02	54.89±0.02	55.1±0.02	59.5±0.03	58.74±0.03
	0.1,1,25	53.44±0.02	**60.01±0.03**	53.9±0.02	53.54±0.02	53.41±0.02	53.66±0.02	58.2±0.03	57.3±0.03
	0.1,2,5	69.66±0.03	**78.42±0.03**	71.22±0.03	70.35±0.04	70.26±0.03	70.93±0.04	77.12±0.03	76.46±0.03
	0.1,2,25	69.04±0.03	75.58±0.03	68.67±0.03	67.88±0.03	67.96±0.04	69.72±0.03	**75.77±0.03**	75.45±0.04
	0.3,1,5	57.62±0.01	**64.11±0.01**	57.81±0.02	57.76±0.01	57.93±0.02	58.64±0.02	58.36±0.02	58.87±0.02
	0.3,1,25	57.0±0.02	**62.16±0.02**	56.18±0.02	56.58±0.02	56.31±0.02	56.79±0.02	58.06±0.02	57.63±0.02
	0.3,2,5	75.54±0.02	**80.98±0.02**	76.0±0.02	75.25±0.02	75.89±0.02	76.77±0.01	76.6±0.01	77.32±0.02
	0.3,2,25	74.48±0.02	**79.31±0.01**	74.51±0.02	74.03±0.02	74.02±0.02	75.09±0.02	75.32±0.02	75.81±0.02
				with **MLP** classifier					
F1-score	0.1,1,5	7.94±0.08	**30.36±0.03**	23.0±0.03	22.9±0.03	23.04±0.03	14.79±0.09	27.05±0.02	25.66±0.02
	0.1,1,25	16.91±0.04	**24.66±0.02**	18.99±0.03	19.52±0.03	18.29±0.03	16.97±0.04	21.31±0.02	20.96±0.02
	0.1,2,5	54.57±0.04	**57.46±0.04**	47.51±0.04	45.43±0.05	50.95±0.05	55.24±0.04	48.86±0.04	45.52±0.04
	0.1,2,25	44.32±0.05	**47.82±0.03**	42.68±0.05	42.35±0.04	44.01±0.04	43.39±0.04	28.84±0.02	30.44±0.04
	0.3,1,5	45.19±0.03	**54.57±0.02**	51.84±0.03	52.37±0.02	51.93±0.02	51.13±0.03	53.66±0.02	53.94±0.02
	0.3,1,25	38.83±0.03	**49.7±0.02**	43.2±0.02	43.64±0.02	42.93±0.02	41.73±0.02	44.64±0.02	44.79±0.02
	0.3,2,5	74.34±0.02	**74.87±0.02**	74.6±0.02	72.14±0.02	72.12±0.02	74.76±0.02	74.58±0.02	74.48±0.01
	0.3,2,25	64.5±0.03	**68.61±0.02**	65.12±0.02	64.71±0.02	64.67±0.03	64.07±0.03	62.69±0.02	62.62±0.03
G-mean	0.1,1,5	10.57±0.09	31.85±0.03	25.22±0.03	25.39±0.03	23.94±0.03	16.82±0.08	**32.26±0.02**	31.53±0.02
	0.1,1,25	17.03±0.04	27.33±0.03	19.5±0.03	20.15±0.03	18.57±0.0 3	17.21±0.04	**27.93±0.02**	27.22±0.02
	0.1,2,5	55.74±0.04	**58.02±0.04**	49.29±0.04	47.57±0.05	51.86±0.05	55.77±0.04	52.72±0.03	50.13±0.03
	0.1,2,25	44.55±0.04	**48.87±0.03**	42.95±0.05	42.62±0.04	44.18±0.04	43.62±0.04	35.61±0.02	36.26±0.04
	0.3,1,5	46.37±0.03	**55.37±0.02**	52.45±0.03	53.42±0.02	52.76±0.02	51.31±0.03	54.64±0.02	54.75±0.02
	0.3,1,25	38.97±0.03	**51.01±0.02**	43.44±0.02	44.01±0.02	43.15±0.02	41.88±0.03	45.63±0.02	45.69±0.03
	0.3,2,5	74.48±0.02	**75.08±0.02**	74.83±0.02	72.85±0.02	72.76±0.02	74.82±0.02	74.88±0.02	74.8±0.01
	0.3,2,25	64.56±0.03	**69.14±0.02**	65.23±0.02	64.82±0.02	64.81±0.03	64.22±0.03	63.53±0.02	63.31±0.03
AUC	0.1,1,5	**71.4±0.03**	71.31±0.03	62.85±0.04	63.04±0.04	64.61±0.04	69.73±0.04	69.32±0.03	67.45±0.03
	0.1,1,25	61.51±0.04	**64.07±0.03**	58.48±0.04	58.53±0.03	57.73±0.04	59.13±0.04	60.73±0.03	59.31±0.04
	0.1,2,5	**90.28±0.01**	89.9±0.02	85.39±0.03	84.09±0.04	86.77±0.03	89.65±0.01	88.72±0.02	87.74±0.02
	0.1,2,25	82.52±0.03	**84.6±0.02**	79.94±0.04	79.77±0.04	80.25±0.04	81.13±0.03	73.5±0.03	74.01±0.05
	0.3,1,5	73.19±0.02	**73.24±0.02**	70.83±0.02	70.01±0.02	70.15±0.0 2	73.0±0.02	72.13±0.02	72.25±0.02
	0.3,1,25	59.87±0.03	**65.94±0.01**	60.88±0.02	61.04±0.02	60.76±0.02	60.62±0.03	60.28±0.02	60.61±0.03
	0.3,2,5	91.2±0.01	**91.22±0.01**	90.68±0.01	89.64±0.02	89.34±0.01	91.01±0.01	90.9±0.01	90.79±0.01
	0.3,2,25	81.84±0.03	**85.69±0.02**	81.81±0.02	81.13±0.03	81.41±0.03	8 0.8±0.03	80.56±0.02	80.42±0.03

Table 13: **F1 score** with **KNN** classifier on KEEL datasets

			Over-sampling			**Under-sampling**		
Dataset	baseline	**LNR**	SMOTE	ADASYN	Borderline	OSS	CC	RUS
1	9.75±0.09	**39.12±0.08**	33.18±0.06	32.05±0.06	34.72±0.07	15.63±0.09	25.67±0.05	19.22±0.04
2	0.17±0.02	**15.19±0.07**	13.13±0.06	13.17±0.06	11.02±0.08	0.35±0.02	8.75±0.03	7.34±0.02
3	26.11±0.14	**43.89±0.11**	36.06±0.07	35.0±0.07	42.49±0.1	31.88±0.13	33.79±0.07	29.54±0.05
4	77.55±0.06	78.29±0.06	**79.57±0.05**	77.64±0.05	78.6±0.05	78.47±0.06	78.22±0.05	78.13±0.05
5	**88.72±0.05**	88.57±0.05	82.39±0.05	77.62±0.06	80.75±0.06	86.17±0.06	84.21±0.06	76.32±0.08
6	60.99±0.1	**69.53±0.08**	62.69±0.08	61.12±0.07	63.1±0.09	66.67±0.09	58.27±0.08	56.72±0.08
7	23.22±0.12	**32.73±0.08**	29.6±0.07	29.72±0.07	29.74±0.07	22.68±0.12	16.58±0.04	23.3±0.05
8	78.36±0.08	80.06±0.07	85.53±0.05	**85.84±0.05**	85.25±0.06	83.59±0.08	82.86±0.06	81.98±0.06
9	72.1±0.05	72.17±0.05	**73.47±0.05**	72.37±0.05	72.85±0.05	71.19±0.06	66.98±0.05	70.93±0.05
10	65.72±0.07	68.51±0.06	68.52±0.06	**69.65±0.06**	69.43±0.06	66.27±0.07	65.31±0.05	67.79±0.06
11	35.23±0.07	**47.75±0.07**	43.48±0.06	43.54±0.07	43.12±0.06	37.7±0.08	39.29±0.07	45.54±0.06
12	65.11±0.09	63.66±0.08	**72.64±0.06**	65.0±0.08	71.17±0.07	64.27±0.1	29.04±0.04	28.22±0.05
13	77.01±0.06	66.98±0.07	**78.78±0.07**	60.15±0.05	62.49±0.05	56.62±0.2	44.23±0.04	38.79±0.07
14	77.05±0.09	**77.45±0.07**	67.07±0.09	68.49±0.1	68.46±0.12	54.9±0.28	54.44±0.07	59.83±0.14
15	86.21±0.09	89.92±0.07	**94.25±0.05**	93.83±0.05	93.72±0.05	90.63±0.06	91.77±0.05	92.2±0.06
16	82.72±0.02	**83.35±0.02**	81.71±0.02	79.93±0.02	82.66±0.02	83.09±0.02	79.22±0.02	77.21±0.02
17	60.36±0.04	**66.88±0.03**	63.54±0.04	63.58±0.03	63.37±0.03	62.02±0.04	61.63±0.04	64.05±0.03
18	52.66±0.05	**64.24±0.04**	61.62±0.03	61.83±0.03	61.9±0.03	57.65±0.05	60.9±0.04	60.57±0.04
19	47.38±0.05	**63.13±0.03**	58.41±0.04	59.71±0.03	58.79±0.03	53.64±0.05	60.11±0.04	59.31±0.03
20	57.96±0.07	**61.61±0.06**	49.79±0.04	45.57±0.04	55.17±0.05	59.6±0.07	42.41±0.06	48.41±0.06
21	**83.07±0.05**	82.74±0.04	69.12±0.04	66.1±0.04	76.65±0.04	83.0±0.05	72.02±0.06	71.15±0.05
22	35.86±0.09	**42.58±0.09**	37.48±0.06	36.5±0.06	41.16±0.07	37.73±0.1	34.31±0.06	34.85±0.06
23	33.27±0.14	47.76±0.09	45.6±0.06	44.28±0.06	**48.52±0.07**	46.52±0.1	41.28±0.06	42.69±0.05
24	5.48±0.09	18.46±0.09	23.88±0.07	21.75±0.08	**30.48±0.1**	11.35±0.12	15.24±0.04	15.34±0.05
25	1.52±0.05	17.42±0.08	19.68±0.06	**20.2±0.06**	18.29±0.09	4.21±0.07	14.44±0.03	13.9±0.03
26	13.4±0.14	33.24±0.1	38.32±0.08	35.12±0.09	**44.6±0.09**	28.01±0.15	31.59±0.07	29.22±0.07
27	75.89±0.07	77.0±0.07	73.9±0.07	72.58±0.07	74.4±0.08	**79.32±0.06**	73.97±0.06	75.16±0.07
28	53.73±0.03	**59.79±0.02**	56.92±0.03	56.41±0.02	56.83±0.02	54.61±0.03	57.76±0.02	57.99±0.03
29	75.66±0.04	**77.96±0.04**	70.65±0.04	68.71±0.04	69.73±0.04	76.64±0.04	63.95±0.04	66.9±0.04
30	18.39±0.1	39.83±0.09	35.38±0.07	35.33±0.07	**41.48±0.08**	27.62±0.12	25.04±0.04	26.66±0.04
31	63.81±0.09	**69.99±0.07**	68.95±0.06	69.31±0.07	68.4±0.07	66.51±0.08	43.87±0.05	44.28±0.06
32	54.57±0.1	56.62±0.1	40.29±0.06	39.92±0.07	52.68±0.09	**57.75±0.1**	24.68±0.05	26.98±0.05

Table 14: **G-mean** with **KNN** classifier on KEEL datasets

			Over-sampling			**Under-sampling**		
Dataset	baseline	**LNR**	SMOTE	ADASYN	Borderline	OSS	CC	RUS
1	16.8±0.13	**39.98±0.08**	35.02±0.06	33.64±0.06	35.21±0.07	22.78±0.11	33.9±0.04	29.95±0.04
2	0.3±0.03	**17.72±0.08**	15.47±0.07	15.52±0.07	11.33±0.08	0.62±0.04	16.2±0.04	15.69±0.03
3	35.35±0.15	**45.11±0.11**	37.61±0.07	36.57±0.08	43.2±0.1	38.32±0.14	36.68±0.07	34.93±0.06
4	78.02±0.06	78.64±0.05	**79.93±0.05**	78.19±0.05	79.1±0.05	78.69±0.06	78.83±0.05	78.78±0.05
5	**88.81±0.05**	88.69±0.05	83.0±0.05	78.55±0.05	81.38±0.05	86.49±0.06	84.75±0.06	77.84±0.07
6	62.17±0.1	**70.18±0.08**	64.55±0.08	62.69±0.07	64.34±0.08	67.19±0.09	62.77±0.06	61.79±0.06
7	26.92±0.13	**34.65±0.08**	30.26±0.07	30.39±0.07	30.49±0.07	27.14±0.12	28.36±0.04	33.2±0.05
8	79.32±0.07	80.48±0.07	85.69±0.05	**86.03±0.05**	85.45±0.06	83.95±0.07	83.33±0.06	82.19±0.06
9	72.54±0.05	73.13±0.05	**74.56±0.05**	73.77±0.04	74.3±0.04	72.03±0.05	70.54±0.04	72.52±0.05
10	66.4±0.07	69.0±0.06	68.77±0.06	**70.14±0.06**	69.78±0.06	66.71±0.07	66.65±0.05	68.16±0.06
11	37.84±0.07	**48.14±0.06**	43.93±0.07	44.18±0.07	43.5±0.06	38.22±0.07	40.41±0.08	46.43±0.07
12	66.82±0.08	64.25±0.08	**73.29±0.06**	65.47±0.08	71.97±0.07	65.6±0.09	40.94±0.04	40.01±0.04
13	78.91±0.05	67.4±0.07	**79.76±0.07**	64.25±0.04	66.2±0.04	59.88±0.17	52.64±0.03	48.16±0.05
14	77.38±0.09	**77.69±0.07**	68.46±0.08	69.54±0.1	69.46±0.11	56.93±0.26	60.03±0.06	63.78±0.11
15	87.24±0.08	90.3±0.06	**94.38±0.05**	94.05±0.04	93.91±0.05	90.98±0.06	92.03±0.05	92.43±0.06
16	82.96±0.02	**83.4±0.02**	82.06±0.02	80.23±0.02	82.83±0.02	83.22±0.02	79.75±0.02	78.29±0.02
17	60.61±0.04	**67.69±0.03**	63.83±0.04	64.18±0.03	63.83±0.03	62.1±0.04	61.84±0.04	64.46±0.04
18	52.86±0.05	**65.51±0.04**	63.14±0.03	63.75±0.03	63.62±0.03	57.85±0.05	62.39±0.04	62.75±0.04
19	48.44±0.05	**64.48±0.03**	59.51±0.04	61.26±0.03	59.98±0.03	53.79±0.04	61.01±0.04	60.92±0.03
20	60.02±0.06	**61.87±0.06**	52.3±0.04	48.07±0.04	56.01±0.05	60.92±0.07	47.18±0.04	51.33±0.05
21	**83.32±0.04**	82.83±0.04	70.91±0.04	68.01±0.04	77.09±0.04	83.17±0.05	73.54±0.05	72.73±0.04
22	41.13±0.09	**43.72±0.09**	39.69±0.06	38.77±0.06	41.99±0.07	41.09±0.09	40.14±0.06	39.82±0.06
23	38.2±0.14	48.45±0.09	47.46±0.07	46.0±0.06	**49.31±0.07**	48.85±0.1	47.4±0.05	48.01±0.05
24	9.2±0.15	20.45±0.1	27.28±0.08	24.81±0.09	**31.51±0.1**	17.44±0.17	24.3±0.04	22.71±0.05
25	2.66±0.08	18.92±0.09	22.55±0.07	22.99±0.07	18.76±0.09	6.78±0.12	**24.16±0.04**	22.47±0.04
26	20.34±0.19	34.85±0.1	40.83±0.08	37.38±0.09	**45.5±0.09**	35.28±0.17	37.91±0.07	35.26±0.07
27	77.69±0.06	77.68±0.06	74.43±0.07	73.05±0.07	74.72±0.07	**80.08±0.06**	74.93±0.06	75.75±0.07
28	54.17±0.03	**61.14±0.03**	57.53±0.03	57.44±0.02	57.62±0.02	54.75±0.03	60.98±0.02	58.96±0.03
29	76.07±0.03	**78.14±0.04**	71.86±0.03	69.83±0.04	70.42±0.04	76.82±0.04	67.64±0.03	69.79±0.04
30	25.64±0.12	40.62±0.09	37.77±0.07	37.52±0.07	**42.05±0.08**	33.46±0.13	35.17±0.04	36.27±0.03
31	65.42±0.09	**70.98±0.06**	70.87±0.06	70.4±0.07	70.09±0.06	67.23±0.08	52.98±0.04	53.26±0.05
32	56.51±0.1	57.36±0.1	44.41±0.06	43.74±0.07	54.07±0.09	**58.86±0.1**	35.55±0.04	37.02±0.05

Table 15: **AUC** with **KNN** classifier on KEEL datasets

			Over-sampling			Under-sampling		
Dataset	baseline	**LNR**	SMOTE	ADASYN	Borderline	OSS	CC	RUS
1	76.65±0.06	87.59±0.05	76.36±0.05	76.22±0.05	74.72±0.05	75.14±0.05	**88.8±0.03**	87.88±0.04
2	61.62±0.07	**72.77±0.08**	63.32±0.07	63.33±0.07	60.68±0.06	61.02±0.06	67.22±0.08	66.47±0.07
3	73.9±0.06	**80.04±0.06**	73.46±0.05	73.11±0.05	74.02±0.06	75.72±0.07	79.71±0.06	79.37±0.05
4	93.26±0.03	92.75±0.03	92.55±0.03	91.46±0.03	91.49±0.03	93.55±0.03	**94.37±0.02**	93.58±0.03
5	95.41±0.03	95.87±0.03	94.81±0.03	93.51±0.03	93.79±0.03	95.98±0.03	**96.22±0.03**	95.48±0.03
6	90.39±0.04	92.06±0.04	89.44±0.04	88.31±0.04	88.45±0.04	91.58±0.04	**93.11±0.03**	92.34±0.04
7	76.73±0.07	77.5±0.07	74.84±0.06	74.9±0.06	75.39±0.05	69.66±0.05	75.12±0.06	**84.29±0.04**
8	94.9±0.03	95.52±0.02	95.36±0.03	95.32±0.03	95.54±0.03	94.91±0.04	**96.3±0.03**	95.1±0.03
9	86.41±0.04	85.46±0.04	**86.66±0.04**	86.15±0.04	86.03±0.04	84.92±0.04	83.92±0.04	84.24±0.04
10	**82.17±0.05**	82.16±0.05	82.08±0.05	82.04±0.05	82.0±0.05	79.83±0.05	80.12±0.05	81.85±0.05
11	63.83±0.05	**67.21±0.05**	62.14±0.05	61.6±0.05	62.16±0.05	61.79±0.05	55.33±0.06	62.51±0.06
12	93.88±0.03	95.36±0.03	95.13±0.03	93.43±0.03	94.87±0.03	93.87±0.04	**97.56±0.01**	96.57±0.01
13	93.47±0.05	93.28±0.05	93.19±0.04	96.33±0.02	95.39±0.03	87.32±0.04	**97.32±0.01**	97.02±0.01
14	90.2±0.04	90.37±0.04	89.0±0.04	89.07±0.04	89.12±0.04	86.4±0.13	**95.45±0.03**	93.35±0.05
15	99.57±0.01	99.41±0.01	**99.59±0.01**	99.52±0.01	99.41±0.01	99.48±0.01	99.58±0.0	99.57±0.01
16	95.53±0.01	95.74±0.01	95.52±0.01	95.18±0.01	95.32±0.01	95.69±0.01	**97.6±0.01**	97.16±0.01
17	77.72±0.03	**79.38±0.03**	75.78±0.03	75.18±0.03	75.05±0.03	76.12±0.03	75.35±0.03	76.92±0.03
18	81.74±0.02	**82.94±0.02**	80.77±0.02	80.77±0.02	80.57±0.02	80.83±0.03	80.53±0.03	79.81±0.03
19	81.26±0.02	**82.42±0.02**	79.47±0.02	79.36±0.02	79.07±0.02	79.85±0.02	81.42±0.02	79.99±0.02
20	83.35±0.04	**84.17±0.03**	82.44±0.03	80.3±0.03	82.63±0.03	82.79±0.03	83.24±0.04	82.46±0.04
21	93.84±0.02	93.99±0.02	92.94±0.02	91.84±0.02	92.96±0.02	93.83±0.02	**94.32±0.02**	93.78±0.02
22	72.94±0.06	75.18±0.06	72.61±0.05	71.68±0.05	72.9±0.05	72.01±0.06	**75.55±0.05**	74.21±0.05
23	78.46±0.06	80.94±0.05	78.03±0.04	77.31±0.04	77.18±0.05	80.21±0.05	**85.6±0.03**	84.94±0.04
24	68.99±0.07	73.35±0.07	70.61±0.07	70.22±0.07	69.37±0.07	69.32±0.07	**75.72±0.07**	70.99±0.08
25	63.51±0.07	64.99±0.07	64.61±0.07	64.7±0.07	64.06±0.07	63.14±0.07	**67.07±0.07**	64.01±0.07
26	73.91±0.06	77.12±0.05	74.1±0.07	73.16±0.06	74.68±0.06	73.81±0.06	**78.95±0.06**	76.07±0.06
27	91.62±0.04	93.15±0.03	92.6±0.03	91.47±0.03	90.9±0.03	95.38±0.03	**97.05±0.01**	96.37±0.02
28	78.04±0.02	**78.67±0.02**	74.32±0.02	73.0±0.02	73.06±0.02	75.61±0.02	76.02±0.02	75.8±0.02
29	93.53±0.02	95.52±0.02	92.83±0.02	91.4±0.02	91.22±0.02	94.22±0.02	**96.67±0.01**	96.51±0.01
30	78.14±0.06	82.78±0.05	77.35±0.05	77.29±0.05	76.76±0.05	78.45±0.05	**90.18±0.03**	89.79±0.03
31	96.56±0.03	**98.27±0.02**	96.48±0.02	96.39±0.02	96.38±0.03	97.14±0.02	98.09±0.01	97.71±0.01
32	86.83±0.05	88.55±0.05	85.65±0.05	85.42±0.05	86.2±0.05	86.96±0.05	**92.84±0.04**	91.89±0.04

Table 16: **F1 score** with **CART** classifier on KEEL datasets

			Over-sampling			**Under-sampling**		
Dataset	baseline	**LNR**	SMOTE	ADASYN	Borderline	OSS	CC	RUS
1	28.61±0.09	**35.51±0.07**	24.22±0.08	23.36±0.07	24.12±0.09	26.04±0.08	18.45±0.04	16.03±0.03
2	6.97±0.08	**10.32±0.06**	8.76±0.07	8.89±0.07	7.08±0.07	6.58±0.06	7.97±0.02	7.26±0.02
3	33.29±0.11	**36.29±0.08**	28.07±0.09	26.85±0.09	31.68±0.1	31.59±0.1	23.55±0.05	23.77±0.06
4	74.28±0.06	**76.71±0.06**	75.73±0.07	75.55±0.06	74.29±0.06	75.61±0.06	75.44±0.07	75.81±0.06
5	73.83±0.07	75.79±0.07	**76.27±0.06**	74.05±0.07	73.94±0.08	71.92±0.08	67.61±0.08	66.14±0.08
6	55.97±0.13	**60.24±0.1**	51.71±0.12	52.56±0.12	51.27±0.12	55.72±0.12	59.2±0.09	56.66±0.09
7	23.25±0.1	**32.35±0.09**	20.44±0.1	20.27±0.09	22.05±0.09	24.11±0.1	10.35±0.03	24.31±0.06
8	85.14±0.06	**87.58±0.06**	85.28±0.06	83.98±0.07	85.35±0.07	78.33±0.1	83.58±0.07	84.74±0.06
9	70.88±0.06	71.61±0.07	71.51±0.07	70.53±0.06	72.13±0.06	**72.59±0.06**	68.87±0.07	71.13±0.07
10	63.32±0.08	65.68±0.08	63.55±0.08	**66.17±0.07**	65.24±0.08	65.11±0.07	65.4±0.07	64.12±0.08
11	37.15±0.07	**48.8±0.06**	37.94±0.08	37.56±0.07	38.18±0.08	40.92±0.07	40.85±0.06	44.37±0.07
12	**78.36±0.06**	73.98±0.05	71.32±0.06	71.39±0.06	70.56±0.06	76.65±0.08	33.87±0.09	50.86±0.08
13	**82.91±0.05**	70.2±0.06	63.46±0.06	61.72±0.05	63.16±0.05	67.22±0.16	58.32±0.04	48.73±0.06
14	76.99±0.07	74.71±0.08	**77.3±0.07**	76.97±0.08	77.11±0.08	75.18±0.08	46.9±0.08	56.99±0.1
15	87.68±0.06	87.86±0.07	92.27±0.06	**92.55±0.05**	92.16±0.05	86.99±0.1	82.02±0.1	86.41±0.09
16	83.7±0.02	**84.6±0.02**	83.12±0.02	80.7±0.02	82.45±0.02	82.8±0.03	66.82±0.04	76.24±0.03
17	57.01±0.05	**64.35±0.03**	58.38±0.04	57.49±0.04	57.05±0.04	58.52±0.04	56.46±0.04	60.28±0.04
18	51.85±0.04	**58.73±0.04**	53.51±0.04	53.66±0.05	52.78±0.05	53.35±0.04	54.65±0.04	57.13±0.04
19	51.7±0.05	**59.4±0.04**	52.88±0.05	52.61±0.05	52.45±0.05	53.62±0.04	54.13±0.05	55.18±0.04
20	49.01±0.07	**54.53±0.06**	48.76±0.07	45.45±0.06	48.47±0.06	47.45±0.07	27.68±0.05	38.24±0.05
21	73.66±0.05	**75.13±0.05**	74.73±0.06	72.41±0.06	74.15±0.05	69.46±0.06	37.73±0.07	57.73±0.07
22	35.41±0.1	**36.02±0.08**	31.54±0.1	28.9±0.08	30.17±0.09	31.76±0.1	24.05±0.04	29.58±0.05
23	40.75±0.09	**47.78±0.08**	42.61±0.09	40.01±0.1	41.73±0.09	43.59±0.09	32.41±0.06	38.92±0.07
24	**23.69±0.12**	19.1±0.09	14.33±0.08	14.97±0.09	17.7±0.1	21.09±0.1	9.9±0.02	11.63±0.04
25	11.82±0.09	**13.91±0.08**	11.12±0.07	10.42±0.08	12.74±0.08	13.22±0.08	12.17±0.02	12.92±0.03
26	**37.61±0.12**	32.78±0.1	27.59±0.11	24.68±0.12	28.67±0.11	33.57±0.11	23.85±0.04	24.35±0.08
27	72.04±0.07	72.59±0.07	**73.13±0.08**	70.52±0.08	70.54±0.08	67.53±0.07	68.77±0.08	72.73±0.07
28	50.46±0.03	**57.79±0.03**	50.98±0.03	50.89±0.03	50.8±0.04	51.74±0.03	53.51±0.03	52.86±0.03
29	68.73±0.05	**76.47±0.04**	71.24±0.05	69.79±0.04	69.76±0.05	70.0±0.05	62.36±0.06	67.41±0.04
30	30.4±0.09	**36.97±0.08**	30.26±0.09	28.75±0.09	28.85±0.09	30.76±0.09	16.71±0.06	24.04±0.04
31	66.19±0.1	68.31±0.08	68.48±0.09	69.24±0.09	**69.48±0.08**	61.56±0.11	55.91±0.1	51.74±0.1
32	41.96±0.11	**47.48±0.09**	44.67±0.11	40.48±0.11	45.22±0.11	38.11±0.11	11.37±0.06	20.25±0.05

Table 17: **G-mean** with **CART** classifier on KEEL datasets

			Over-sampling			**Under-sampling**		
Dataset	baseline	**LNR**	SMOTE	ADASYN	Borderline	OSS	CC	RUS
1	28.91±0.09	**37.02±0.08**	24.49±0.08	23.64±0.07	24.34±0.09	26.53±0.08	26.61±0.04	25.34±0.04
2	7.07±0.08	12.23±0.07	9.05±0.07	9.22±0.07	7.23±0.08	6.82±0.06	14.67±0.04	**15.17±0.04**
3	33.71±0.11	**37.26±0.09**	28.36±0.09	27.08±0.09	32.23±0.1	32.46±0.1	28.62±0.06	30.74±0.07
4	74.51±0.06	**77.06±0.06**	75.9±0.07	75.76±0.06	74.49±0.06	75.85±0.06	75.81±0.07	76.35±0.06
5	74.25±0.07	76.23±0.06	**76.63±0.06**	74.39±0.07	74.23±0.08	72.82±0.07	68.85±0.08	68.13±0.07
6	56.92±0.13	60.96±0.1	52.37±0.12	53.25±0.12	51.95±0.12	56.59±0.12	**60.99±0.09**	59.45±0.08
7	25.63±0.1	**34.26±0.09**	21.25±0.1	20.93±0.1	22.74±0.09	25.93±0.1	21.69±0.03	32.67±0.05
8	85.49±0.06	**87.81±0.06**	85.59±0.06	84.28±0.07	85.63±0.07	78.97±0.09	83.89±0.07	85.05±0.06
9	71.18±0.06	72.02±0.07	71.81±0.06	70.82±0.06	72.54±0.06	**72.88±0.06**	69.45±0.07	71.58±0.07
10	63.62±0.08	65.99±0.08	63.88±0.08	**66.48±0.07**	65.51±0.08	65.62±0.07	65.82±0.07	64.5±0.08
11	37.38±0.07	**49.54±0.06**	38.1±0.08	37.72±0.07	38.36±0.08	41.32±0.07	42.43±0.06	45.59±0.07
12	**78.88±0.05**	74.87±0.04	71.95±0.06	71.98±0.06	71.24±0.06	77.19±0.07	44.89±0.07	58.07±0.06
13	**84.21±0.04**	70.64±0.06	66.67±0.04	65.64±0.04	66.7±0.04	69.37±0.15	64.16±0.03	56.51±0.05
14	77.31±0.07	75.22±0.08	**77.67±0.07**	77.37±0.07	77.49±0.08	75.77±0.08	53.31±0.06	60.6±0.08
15	87.95±0.06	88.16±0.06	92.41±0.06	**92.71±0.05**	92.34±0.05	87.68±0.09	83.41±0.09	86.92±0.08
16	83.74±0.02	**84.7±0.02**	83.16±0.02	80.74±0.02	82.47±0.02	82.91±0.03	69.36±0.03	77.57±0.03
17	57.1±0.05	**64.96±0.03**	58.46±0.04	57.59±0.04	57.13±0.04	58.69±0.04	56.67±0.04	60.61±0.04
18	51.97±0.04	**59.44±0.05**	53.58±0.04	53.73±0.05	52.89±0.05	53.54±0.04	55.72±0.04	58.26±0.04
19	51.81±0.05	**60.38±0.04**	52.98±0.05	52.71±0.05	52.54±0.05	53.86±0.04	55.31±0.05	56.34±0.04
20	49.32±0.07	**55.0±0.06**	49.06±0.07	45.71±0.06	48.71±0.06	47.83±0.07	35.91±0.05	43.62±0.04
21	73.83±0.05	**75.5±0.05**	74.92±0.06	72.64±0.06	74.31±0.05	69.98±0.06	46.06±0.05	61.46±0.06
22	35.73±0.1	**36.82±0.08**	31.91±0.1	29.26±0.08	30.45±0.09	32.25±0.1	32.9±0.05	34.84±0.05
23	41.2±0.09	**48.5±0.08**	43.01±0.09	40.4±0.1	42.16±0.09	44.25±0.09	39.88±0.06	43.41±0.07
24	**24.18±0.12**	20.31±0.09	14.63±0.08	15.32±0.09	18.05±0.1	21.76±0.1	19.18±0.04	19.26±0.05
25	12.08±0.09	15.06±0.08	11.37±0.08	10.62±0.08	12.92±0.08	13.73±0.09	**21.99±0.04**	20.6±0.05
26	**38.18±0.12**	33.67±0.1	28.07±0.11	24.99±0.12	29.19±0.11	34.46±0.11	32.44±0.05	30.63±0.08
27	72.45±0.07	73.01±0.07	**73.55±0.08**	70.9±0.08	71.1±0.07	70.52±0.06	70.89±0.07	73.09±0.07
28	50.5±0.03	**58.81±0.03**	51.04±0.03	50.95±0.03	50.84±0.04	51.87±0.03	55.16±0.03	53.73±0.03
29	68.86±0.05	**76.95±0.04**	71.36±0.05	69.93±0.04	69.86±0.05	70.2±0.05	65.7±0.05	69.63±0.03
30	30.8±0.09	**38.13±0.08**	30.59±0.09	29.08±0.09	29.19±0.1	31.16±0.09	27.67±0.06	33.14±0.05
31	66.73±0.1	69.04±0.08	68.91±0.09	69.71±0.08	**70.01±0.08**	62.22±0.11	60.96±0.08	58.02±0.08
32	42.54±0.11	**48.97±0.09**	45.49±0.11	41.12±0.11	45.83±0.11	39.04±0.12	22.69±0.05	30.39±0.05

Table 18: **AUC** with **CART** classifier on KEEL datasets

			Over-sampling			Under-sampling		
Dataset	baseline	**LNR**	SMOTE	ADASYN	Borderline	OSS	CC	RUS
1	62.85±0.05	72.47±0.06	61.97±0.05	61.45±0.05	60.98±0.05	63.12±0.05	74.83±0.05	**74.89±0.05**
2	52.45±0.04	57.64±0.06	53.92±0.04	54.09±0.05	52.6±0.04	52.54±0.04	61.73±0.08	**61.8±0.08**
3	63.71±0.06	**68.64±0.06**	61.82±0.05	61.03±0.05	63.05±0.05	65.25±0.06	66.11±0.06	68.44±0.07
4	82.33±0.04	85.27±0.04	83.57±0.05	83.57±0.05	82.46±0.04	84.36±0.05	84.64±0.05	**85.42±0.04**
5	84.23±0.05	**86.4±0.05**	86.19±0.05	84.76±0.05	84.52±0.06	85.83±0.05	84.06±0.05	84.26±0.05
6	74.04±0.08	79.37±0.07	72.69±0.08	73.06±0.07	72.03±0.07	77.02±0.08	**82.51±0.06**	82.4±0.06
7	64.23±0.09	73.74±0.1	63.72±0.09	63.35±0.1	63.77±0.1	64.48±0.09	55.67±0.08	**77.43±0.07**
8	89.1±0.05	**91.81±0.05**	89.53±0.05	88.7±0.06	89.63±0.05	86.07±0.07	88.26±0.05	90.62±0.05
9	77.11±0.05	77.5±0.05	77.59±0.05	76.83±0.05	78.14±0.05	**78.31±0.05**	74.78±0.06	77.03±0.05
10	70.72±0.06	71.97±0.06	70.76±0.06	**72.71±0.05**	72.04±0.06	70.86±0.06	71.37±0.06	70.23±0.07
11	56.22±0.04	**62.71±0.05**	56.45±0.05	56.22±0.05	56.59±0.05	57.06±0.05	53.7±0.05	57.83±0.06
12	95.71±0.03	**97.0±0.03**	96.17±0.03	96.09±0.03	96.11±0.03	96.1±0.03	92.78±0.02	96.42±0.02
13	**99.29±0.0**	98.82±0.0	99.23±0.0	99.15±0.01	99.2±0.0	98.45±0.01	99.01±0.0	97.55±0.01
14	88.28±0.05	87.94±0.05	**88.79±0.05**	88.77±0.05	88.61±0.06	88.6±0.05	82.94±0.05	85.71±0.05
15	91.59±0.04	93.18±0.04	94.8±0.04	**94.98±0.04**	94.61±0.04	94.4±0.04	93.5±0.04	93.84±0.05
16	90.6±0.01	93.01±0.01	91.32±0.01	89.96±0.01	90.41±0.02	91.79±0.01	90.53±0.01	**93.48±0.01**
17	66.32±0.03	**70.74±0.03**	67.02±0.03	66.01±0.03	65.8±0.03	66.59±0.03	64.58±0.03	67.5±0.03
18	66.9±0.03	**72.06±0.03**	67.99±0.03	68.09±0.03	67.56±0.04	67.8±0.03	68.71±0.03	70.83±0.03
19	67.22±0.03	**73.32±0.04**	68.0±0.04	67.79±0.03	67.69±0.03	68.49±0.03	68.91±0.04	69.81±0.03
20	71.39±0.04	**76.59±0.04**	72.18±0.04	70.06±0.04	71.37±0.04	72.02±0.05	64.33±0.06	73.68±0.04
21	85.67±0.04	**88.61±0.03**	86.26±0.04	85.69±0.04	85.83±0.04	85.66±0.04	76.17±0.04	86.43±0.03
22	63.38±0.05	**65.27±0.06**	61.89±0.06	60.26±0.05	60.77±0.05	62.24±0.06	57.03±0.07	63.97±0.05
23	66.57±0.06	72.64±0.06	68.17±0.05	66.89±0.07	67.37±0.06	70.04±0.06	69.05±0.06	**72.65±0.06**
24	60.66±0.07	59.76±0.06	56.05±0.05	56.64±0.06	57.45±0.06	60.67±0.06	59.3±0.07	**61.3±0.08**
25	53.5±0.04	55.84±0.06	53.33±0.05	52.78±0.05	54.03±0.05	54.68±0.05	57.72±0.06	**58.25±0.07**
26	65.67±0.06	65.17±0.07	61.09±0.06	59.37±0.07	61.23±0.06	65.56±0.07	**66.99±0.06**	64.76±0.08
27	83.21±0.05	84.5±0.05	84.85±0.06	83.08±0.05	84.98±0.05	**91.27±0.04**	90.02±0.04	85.93±0.05
28	64.57±0.02	**69.38±0.02**	64.82±0.02	64.68±0.02	64.66±0.03	65.09±0.02	65.14±0.02	65.11±0.03
29	82.02±0.03	**90.02±0.03**	84.43±0.03	83.7±0.03	83.03±0.04	84.29±0.03	88.34±0.02	89.59±0.02
30	63.47±0.05	71.58±0.05	64.71±0.06	63.99±0.05	62.94±0.05	65.01±0.05	72.15±0.09	**78.74±0.06**
31	81.08±0.06	87.63±0.06	83.63±0.06	84.11±0.06	83.94±0.06	82.18±0.07	93.35±0.04	**93.72±0.03**
32	70.93±0.06	78.97±0.07	74.56±0.07	71.76±0.07	73.45±0.07	71.48±0.07	71.71±0.05	**81.01±0.05**

Table 19: **F1 score** with **MLP** classifier on KEEL datasets

			Over-sampling			**Under-sampling**		
Dataset	baseline	**LNR**	SMOTE	ADASYN	Borderline	OSS	CC	RUS
1	26.47±0.12	**44.35±0.08**	37.11±0.07	36.81±0.06	38.36±0.07	32.04±0.13	27.03±0.04	24.62±0.05
2	0.0±0.0	**18.4±0.07**	13.8±0.07	12.75±0.07	10.29±0.07	0.0±0.0	10.04±0.03	8.93±0.02
3	44.83±0.17	**52.22±0.08**	48.33±0.08	45.94±0.09	51.69±0.09	43.47±0.21	40.43±0.07	36.91±0.06
4	75.16±0.07	76.18±0.06	**77.05±0.05**	76.63±0.06	76.75±0.05	75.48±0.07	76.83±0.04	76.13±0.05
5	82.01±0.06	**82.46±0.06**	81.27±0.07	76.19±0.07	76.7±0.08	80.06±0.06	78.89±0.06	75.15±0.07
6	40.44±0.31	**66.92±0.08**	66.48±0.09	66.17±0.08	66.07±0.09	60.85±0.11	61.47±0.07	59.16±0.08
7	21.49±0.11	**31.02±0.1**	27.75±0.06	26.45±0.07	27.55±0.07	20.89±0.12	16.94±0.06	25.17±0.05
8	86.35±0.05	86.15±0.06	87.07±0.06	87.02±0.06	**88.18±0.05**	83.64±0.07	85.72±0.06	87.44±0.05
9	51.91±0.31	71.02±0.08	69.46±0.1	**72.28±0.07**	69.79±0.1	59.72±0.27	69.43±0.07	70.44±0.06
10	63.87±0.07	64.83±0.06	64.16±0.07	65.06±0.07	**66.22±0.07**	63.52±0.08	64.27±0.06	65.75±0.07
11	29.54±0.12	**50.44±0.07**	48.06±0.08	48.31±0.07	48.0±0.08	43.26±0.08	40.48±0.07	47.47±0.08
12	**68.6±0.07**	66.18±0.05	63.01±0.06	62.55±0.05	64.46±0.05	67.3±0.09	50.6±0.05	45.61±0.07
13	**79.55±0.05**	70.58±0.07	53.64±0.05	55.36±0.06	56.74±0.05	69.39±0.16	51.48±0.06	49.38±0.06
14	45.53±0.34	70.19±0.09	72.12±0.09	70.46±0.1	71.65±0.1	**73.86±0.11**	58.99±0.1	56.48±0.11
15	94.3±0.04	95.24±0.04	95.02±0.03	95.31±0.04	**95.4±0.03**	93.34±0.05	93.31±0.05	94.07±0.05
16	82.79±0.02	83.65±0.02	81.57±0.02	76.76±0.03	80.04±0.02	**84.15±0.02**	77.06±0.03	77.85±0.02
17	61.88±0.04	**67.36±0.03**	64.76±0.04	64.84±0.03	64.85±0.03	63.81±0.04	61.75±0.04	64.79±0.04
18	71.16±0.04	**73.2±0.03**	72.2±0.04	71.87±0.03	71.46±0.03	71.74±0.04	71.43±0.03	70.93±0.04
19	62.11±0.05	**67.23±0.04**	66.9±0.04	66.66±0.04	67.18±0.04	62.68±0.08	65.18±0.04	64.96±0.04
20	54.87±0.1	**59.41±0.06**	47.81±0.06	40.61±0.06	50.05±0.08	55.88±0.08	37.26±0.05	38.22±0.05
21	78.8±0.06	**79.8±0.05**	72.59±0.05	65.8±0.08	69.04±0.1	78.71±0.05	59.3±0.08	65.77±0.09
22	32.23±0.1	**40.73±0.09**	35.86±0.08	31.63±0.09	38.56±0.1	31.22±0.13	31.61±0.06	30.49±0.07
23	44.73±0.12	**50.94±0.08**	48.17±0.1	47.13±0.1	48.43±0.09	45.08±0.13	41.05±0.06	38.67±0.08
24	0.0±0.0	16.27±0.08	16.75±0.09	15.27±0.09	**22.28±0.13**	1.5±0.04	12.14±0.04	11.28±0.04
25	0.0±0.0	**18.43±0.09**	14.18±0.08	14.0±0.08	13.09±0.09	0.1±0.01	15.63±0.05	13.42±0.03
26	8.76±0.15	33.8±0.09	29.75±0.08	**39.72±0.1**	25.94±0.14	30.1±0.06	26.53±0.07	28.76±0.11
27	69.77±0.08	71.14±0.08	68.47±0.07	**71.24±0.08**	70.84±0.08	67.36±0.08	64.6±0.07	61.41±0.08
28	55.49±0.03	**60.34±0.03**	59.53±0.03	59.0±0.02	59.16±0.02	58.09±0.03	58.9±0.02	59.75±0.02
29	78.32±0.04	**78.37±0.04**	75.25±0.03	73.47±0.04	75.53±0.04	78.23±0.04	69.79±0.04	69.39±0.04
30	10.44±0.13	**41.68±0.07**	36.45±0.08	36.55±0.07	38.78±0.07	19.53±0.15	24.72±0.04	22.67±0.04
31	60.93±0.11	66.58±0.08	**74.58±0.07**	74.19±0.07	73.77±0.08	67.37±0.1	52.98±0.08	45.92±0.07
32	49.7±0.16	**58.02±0.1**	46.87±0.1	45.48±0.1	54.62±0.11	49.75±0.15	26.67±0.07	22.41±0.05

Table 20: **G-mean** with **MLP** classifier on KEEL datasets

			Over-sampling			**Under-sampling**		
Dataset	baseline	**LNR**	SMOTE	ADASYN	Borderline	OSS	CC	RUS
1	31.86±0.13	**45.44±0.08**	40.6±0.07	40.53±0.06	40.25±0.07	35.08±0.14	35.94±0.04	34.36±0.04
2	0.0±0.0	**20.99±0.08**	15.88±0.08	14.55±0.08	10.62±0.08	0.0±0.0	17.33±0.04	17.66±0.04
3	47.07±0.18	**53.11±0.08**	49.47±0.08	47.01±0.09	52.21±0.09	44.74±0.22	46.3±0.06	43.42±0.06
4	75.52±0.07	76.73±0.06	77.5±0.05	77.25±0.06	77.44±0.05	75.77±0.07	**77.63±0.04**	77.16±0.05
5	82.24±0.06	**82.73±0.06**	81.55±0.07	76.7±0.07	77.11±0.08	80.42±0.06	79.6±0.06	76.35±0.07
6	40.92±0.31	**67.82±0.08**	67.24±0.08	66.9±0.08	66.79±0.09	61.3±0.11	63.87±0.07	62.48±0.07
7	26.88±0.12	32.6±0.1	30.15±0.07	28.9±0.07	29.85±0.08	25.56±0.13	24.64±0.06	**33.28±0.05**
8	86.56±0.05	86.37±0.06	87.28±0.06	87.22±0.06	**88.35±0.05**	84.04±0.07	85.92±0.05	87.74±0.05
9	52.19±0.32	71.64±0.08	70.09±0.1	**73.03±0.07**	70.7±0.1	60.08±0.27	70.03±0.07	70.98±0.06
10	64.33±0.07	65.13±0.06	64.42±0.07	65.51±0.07	**66.52±0.07**	64.05±0.07	64.77±0.06	66.14±0.07
11	34.05±0.11	**50.69±0.07**	48.41±0.08	48.85±0.08	48.38±0.08	44.05±0.08	42.18±0.07	48.17±0.08
12	**69.45±0.06**	66.84±0.05	66.88±0.05	65.98±0.04	68.09±0.04	68.24±0.09	57.81±0.04	53.89±0.05
13	**81.33±0.04**	70.94±0.06	59.41±0.04	60.61±0.04	61.87±0.04	71.22±0.15	57.92±0.04	56.22±0.04
14	45.94±0.34	70.61±0.09	72.67±0.09	71.04±0.1	72.16±0.1	**74.31±0.11**	61.41±0.09	59.95±0.1
15	94.42±0.04	95.41±0.04	95.11±0.03	95.41±0.04	**95.49±0.03**	93.52±0.05	93.59±0.04	94.28±0.05
16	82.97±0.02	83.69±0.02	82.29±0.02	78.08±0.03	80.81±0.02	**84.2±0.02**	78.03±0.02	79.13±0.02
17	62.12±0.04	**67.97±0.03**	65.02±0.04	65.3±0.03	65.25±0.03	63.95±0.04	61.94±0.04	65.25±0.04
18	71.28±0.04	**73.91±0.03**	72.49±0.04	72.3±0.03	71.91±0.03	72.04±0.04	72.0±0.03	71.73±0.04
19	62.31±0.05	**68.17±0.04**	67.31±0.04	67.1±0.04	67.65±0.04	63.07±0.07	66.0±0.04	65.98±0.04
20	56.8±0.09	**59.73±0.06**	48.89±0.06	42.18±0.06	50.57±0.07	57.06±0.08	41.4±0.05	43.0±0.05
21	79.19±0.05	**79.94±0.05**	72.92±0.05	66.3±0.08	69.36±0.1	79.01±0.05	61.82±0.07	67.78±0.08
22	37.12±0.09	**41.32±0.09**	36.55±0.08	32.3±0.1	39.21±0.1	32.61±0.13	35.08±0.07	34.97±0.07
23	46.79±0.12	**51.6±0.08**	48.65±0.1	47.58±0.1	48.87±0.09	46.21±0.12	44.05±0.06	42.76±0.07
24	0.0±0.0	18.09±0.09	17.89±0.09	16.36±0.09	**23.63±0.13**	1.79±0.05	19.57±0.05	18.63±0.05
25	0.0±0.0	19.33±0.09	14.83±0.08	14.61±0.08	13.9±0.1	0.1±0.01	**21.75±0.06**	20.38±0.05
26	9.76±0.16	36.43±0.1	31.83±0.08	**41.08±0.11**	26.77±0.15	36.99±0.06	33.3±0.07	29.85±0.11
27	70.63±0.08	71.56±0.08	68.93±0.07	**71.71±0.08**	71.32±0.08	67.92±0.08	66.34±0.07	63.68±0.08
28	56.16±0.03	60.79±0.03	60.29±0.03	60.34±0.02	60.43±0.02	58.27±0.03	**61.04±0.02**	60.76±0.02
29	78.42±0.04	**78.6±0.04**	75.82±0.03	74.14±0.04	75.93±0.04	78.37±0.04	72.07±0.04	71.61±0.04
30	12.52±0.15	**42.27±0.07**	38.54±0.08	38.64±0.08	39.47±0.07	21.23±0.16	32.73±0.05	31.65±0.04
31	61.89±0.11	67.53±0.08	**74.92±0.07**	74.56±0.07	74.13±0.08	67.93±0.1	58.84±0.07	53.74±0.06
32	52.58±0.16	**58.58±0.1**	48.4±0.1	46.77±0.1	55.06±0.11	51.87±0.14	34.56±0.06	32.06±0.05

Table 21: **AUC** with **MLP** classifier on KEEL datasets

			Over-sampling			Under-sampling		
Dataset	baseline	**LNR**	SMOTE	ADASYN	Borderline	OSS	CC	RUS
1	**92.5±0.02**	92.24±0.03	89.24±0.05	89.12±0.05	88.18±0.05	90.38±0.04	91.48±0.04	91.19±0.04
2	**79.15±0.06**	78.32±0.06	70.78±0.08	70.43±0.07	68.96±0.09	78.62±0.06	72.97±0.05	72.24±0.06
3	**91.61±0.03**	91.18±0.04	88.8±0.05	88.29±0.05	90.67±0.04	90.64±0.04	90.31±0.03	89.0±0.04
4	93.75±0.03	93.68±0.03	**94.27±0.02**	94.04±0.02	94.0±0.02	93.0±0.03	94.01±0.02	93.83±0.02
5	94.94±0.03	**95.52±0.03**	95.35±0.03	94.45±0.03	93.65±0.03	94.71±0.03	95.48±0.03	94.91±0.03
6	**91.21±0.05**	90.85±0.05	90.46±0.04	90.12±0.05	90.28±0.05	88.4±0.05	89.54±0.04	89.56±0.04
7	**84.62±0.05**	83.95±0.06	72.55±0.08	70.23±0.09	75.84±0.08	81.81±0.07	70.75±0.08	81.56±0.07
8	96.62±0.03	96.6±0.03	97.25±0.03	97.21±0.03	**97.7±0.03**	95.76±0.03	95.56±0.04	97.05±0.03
9	76.43±0.14	82.25±0.06	83.99±0.06	**84.16±0.05**	81.87±0.08	78.04±0.14	81.94±0.05	81.92±0.05
10	75.21±0.05	75.25±0.05	75.26±0.05	75.35±0.06	**76.05±0.05**	73.33±0.06	75.56±0.05	74.92±0.06
11	66.32±0.05	**67.94±0.05**	66.83±0.06	66.1±0.06	66.52±0.07	65.88±0.06	56.31±0.07	64.09±0.08
12	98.79±0.0	98.78±0.0	**98.93±0.01**	98.46±0.01	98.73±0.01	98.7±0.01	98.7±0.0	98.38±0.01
13	98.56±0.01	98.57±0.01	**98.71±0.0**	97.6±0.01	98.53±0.01	97.19±0.03	98.6±0.01	98.39±0.01
14	93.18±0.03	93.24±0.03	93.73±0.03	**93.99±0.03**	93.86±0.03	90.97±0.05	92.35±0.03	92.18±0.04
15	**99.89±0.0**	99.87±0.0	99.86±0.0	99.86±0.0	99.87±0.0	99.64±0.01	**99.89±0.0**	99.82±0.0
16	98.12±0.01	98.11±0.01	**98.52±0.0**	97.86±0.01	97.87±0.01	98.13±0.01	97.94±0.01	98.05±0.01
17	79.94±0.03	**80.48±0.03**	78.43±0.03	77.87±0.03	77.31±0.03	79.05±0.03	76.55±0.03	78.07±0.03
18	90.88±0.02	90.47±0.02	**90.96±0.02**	89.94±0.02	89.23±0.02	90.45±0.02	89.97±0.02	89.27±0.03
19	**88.29±0.02**	87.52±0.02	88.1±0.02	87.67±0.02	88.08±0.02	85.98±0.05	86.61±0.02	86.21±0.02
20	**83.13±0.04**	82.15±0.04	79.59±0.04	77.41±0.04	79.86±0.05	82.64±0.04	76.89±0.04	78.63±0.04
21	**93.14±0.03**	92.9±0.03	91.89±0.03	90.74±0.03	90.11±0.04	92.89±0.03	90.63±0.03	92.64±0.03
22	**75.1±0.06**	74.29±0.07	71.19±0.05	68.97±0.07	72.3±0.07	71.76±0.07	69.19±0.07	69.25±0.06
23	82.02±0.05	81.43±0.06	**82.2±0.07**	81.74±0.07	80.97±0.06	78.79±0.06	78.35±0.05	77.88±0.06
24	71.04±0.07	**72.42±0.07**	68.17±0.08	67.31±0.07	67.02±0.08	70.46±0.08	67.27±0.07	65.72±0.08
25	63.88±0.06	66.21±0.07	64.37±0.07	63.99±0.07	60.52±0.07	62.66±0.07	**66.55±0.07**	62.4±0.07
26	76.47±0.06	78.45±0.06	76.34±0.05	79.14±0.06	74.53±0.06	**79.95±0.05**	74.65±0.07	75.44±0.06
27	91.66±0.04	91.05±0.05	91.02±0.04	91.31±0.05	91.16±0.05	90.98±0.05	**92.35±0.04**	91.85±0.04
28	**79.64±0.02**	79.37±0.02	78.49±0.02	77.93±0.02	77.5±0.02	79.43±0.02	77.52±0.02	78.69±0.02
29	97.13±0.01	**97.26±0.01**	96.31±0.01	95.56±0.01	95.74±0.02	96.84±0.01	96.58±0.01	96.38±0.01
30	**87.09±0.04**	86.62±0.04	85.54±0.05	86.08±0.05	84.54±0.05	84.0±0.05	84.29±0.05	82.39±0.05
31	98.37±0.01	98.16±0.01	**98.4±0.01**	98.29±0.01	98.2±0.01	97.88±0.02	97.68±0.01	97.59±0.01
32	**92.34±0.04**	92.28±0.04	89.45±0.04	90.47±0.03	90.88±0.04	90.58±0.05	88.94±0.04	89.41±0.04